

## Review

## Strain alignment of conjugated polymers: Method, microstructure, and applications

Harry M. Schrickx,<sup>1</sup> Pratik Sen,<sup>1</sup> Nrup Balar,<sup>1,2</sup> and Brendan T. O'Connor<sup>1,\*</sup>

## SUMMARY

Straining conjugated polymer films is an effective strategy for controlling molecular orientation. Aligning polymer chains within the film plane significantly influences both electrical and optical properties, thereby presenting avenues for improving electronic device performance and unlocking novel device functionalities. The unique anisotropic optoelectronic nature of these films opens up possibilities for enhanced charge mobility as well as innovative applications in optical sensing and light emission. A polymer film's response to strain also provides practical information on its mechanical properties and potential for implementation in flexible and stretchable applications. This review delves into the process of strain alignment of conjugated polymers, mechanical considerations, morphological analysis, and devices applications. The exploration begins with a concise overview of various polymer alignment processing methods, followed by an in-depth examination of strain alignment and transfer printing techniques employed in device fabrication. We then discuss molecular characteristics that support polymer ductility and strain alignment. Accurately characterizing the microstructure of aligned films is then reviewed. Finally, we present an overview of device demonstrations that have utilized strain-aligned conjugated polymer films.

## INTRODUCTION

Straining conjugated polymer films has been shown to effectively align the polymer backbone in the plane of the film. This alignment can enhance charge mobility ( $\mu$ ) in organic field-effect transistors (OFETs)<sup>1</sup> and introduce intrinsic polarization in sensitive organic photodetectors (OPDs)<sup>2</sup> and polarized light emission in organic light emitting diodes (OLEDs).<sup>3</sup> Beyond these optoelectronic applications, strain alignment can also provide insight into molecular packing and thermomechanical behavior of the polymer. The practice of driving molecular alignment in polymer films through strain is not a recent development. To see some of the earliest works of strain alignment, we must go back nearly 100 years to Land-Wheelwright Laboratories. Edwin Land is best known as co-founder of the Polaroid Corporation and the Polaroid instant camera, but the foundation for this work came several years earlier in his development of inexpensive polarizing films (Figure 1).<sup>4</sup> His first patent for a polarizing film involved orienting herapathite crystals embedded in a transparent polymer film through the application of a magnetic field.<sup>5</sup> However, years later, he invented a polarizing film made by stretching polyvinyl alcohol (PVA). The PVA was strained between 225% and 800% to uniaxially align the polymer chains that were subsequently dyed with polyiodide. The film's dichroic ratio (the ratio between absorbance of linearly polarized light oriented parallel and perpendicular to the direction of alignment [DR]) was approximately 90, making it an excellent polarizer.<sup>6,7</sup>

<sup>1</sup>Department of Mechanical and Aerospace Engineering and Organic and Carbon Electronics Laboratories (ORaCEL), North Carolina State University, Raleigh, NC 27695, USA

<sup>2</sup>Department of Physics and ORaCEL, North Carolina State University, Raleigh, NC 27695, USA

\*Correspondence: [btoconno@ncsu.edu](mailto:btoconno@ncsu.edu)  
<https://doi.org/10.1016/j.xcrp.2024.102076>



A more robust polarizing film was later developed based on a strain-aligned PVA-polyvinylene block copolymer, known as K-sheet polarizers.<sup>8,9</sup> This process led to DRs exceeding 80 along with improved moisture resistance.<sup>10</sup> Polaroid-type polarizers are among the most common seen today, with applications in sunglasses, optical filters, and liquid crystal displays.

In early research on conducting polymers, films were strained to manage the polymer morphology and electrical properties. In 1986, strain alignment was used to increase the electrical conductivity of polypyrrole along the direction of strain.<sup>11,12</sup> A few years later, strain-aligned poly(3-octylthiophene) was reported showing polymer chain alignment and charge mobility anisotropy.<sup>13–15</sup> More recently, Goffri et al. and Muller et al. demonstrated the ability to apply large strains to poly(3-hexylthiophene) (P3HT) blended with polyethylene without film rupture.<sup>16,17</sup> These demonstrations of strain-aligned conjugated polymers were conducted for bulk samples, with thicknesses of 0.5–2  $\mu\text{m}$  (Figure 1).<sup>16,17</sup> However, many organic electronic devices rely on having thin films with thickness less than 200 nm. Strain alignment of these thin films relies on straining while on a supporting substrate. The most common approach today is to strain the conjugated polymer film while on an elastomer such as polydimethylsiloxane (PDMS). In this approach, the film on a PDMS stack is strained, and then the polymer thin film is transfer printed to a receiving substrate as part of device fabrication or for morphological characterization.<sup>1,18</sup>

Aligning polymer chains through strain has many benefits compared to other alignment strategies. One key aspect of strain alignment is the ability to precisely vary alignment through the magnitude of applied strain. Strained films typically show a linear correlation between the applied strain and the degree of in-plane alignment captured by the DR.<sup>1,2</sup> The added level of control is advantageous in applications where consistent alignment is required across a set of devices (e.g., polarized photodetectors).<sup>19,20</sup> In contrast to other solid-state and solution assembly alignment strategies, strain alignment is not influenced by film thickness. Strain alignment avoids any gradient of alignment or morphology through the film thickness or across the film area. Strained films are also easily transferred to a wide range of receiving substrates and electronic device architectures. Thus, the approach is compatible with a broad range of characterization methods that may not be accessible with other alignment strategies. Additionally, strain alignment has the ability to scale to meet the demand of larger area applications. This is evident across the plastics industry, where strained films are used in high-throughput manufacturing to optimize mechanical, thermal, and optical properties.<sup>21</sup> It is important to note that straining polymer semiconductors while on elastomer supports has gained significant recent attention due to the interest in developing intrinsically stretchable organic electronic devices. A film's response to strain is fundamental to stretchable electronics, and there is a clear need to better understand strain-dependent morphological changes. For more in-depth focus on stretchable electronic materials, devices, and applications, we refer the reader to other reviews on this subject.<sup>22–24</sup> Here, we focus on the method, morphology, and applications of strain-aligned films transfer printed from the elastomer onto a non-stretchable receiving substrate. However, we include important overlapping considerations including mechanical behavior and morphological analysis of target polymers that are directly applicable to stretchable organic electronics.

Our review focuses on the application of strain to align conjugated polymer films in the plane of the film, characterizing the morphological changes accompanying the strain process, and device applications of the strain-aligned films. We begin with a

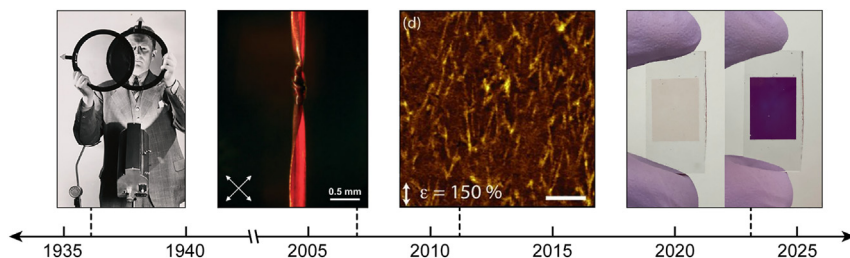


**Figure 1. Timeline of polymer film strain alignment with a focus on polymer semiconductors**  
From left to right: George Wheelwright III demonstrating Polaroid polarizing lenses in 1936.<sup>32</sup> Strain-oriented P3HT-polyethylene block copolymer film tied in a knot (2007). Reproduced with permission.<sup>17</sup> Copyright 2007, John Wiley and Sons. AFM image of a P3HT film strained 150% exhibiting fibrils in the direction of strain (2011), scale bar: 2  $\mu\text{m}$ . Reproduced with permission.<sup>1</sup> Copyright 2011, John Wiley and Sons. Image of strain-aligned PBnDT-FTAZ film with perpendicular (left) and parallel (right) polarized light.<sup>30</sup>

brief comparison of strain alignment to other alignment strategies, considering the benefits of each approach. We then delve deeper into the strain alignment process, considering the transfer of an oriented film to a receiving substrate. We then discuss the molecular features and associated thermomechanical behavior that provide insight into the polymer's response to strain. This is followed by reviewing common strategies used to probe molecular orientation and morphology in aligned films and best practices for measurement interpretation. Lastly, we review recent reports of applications that employ strain-aligned conjugated polymer films. In summary, this review provides a comprehensive overview of strain alignment and the opportunities this approach has in advancing organic electronics.

### Alignment strategies

Uniaxial alignment of conjugated polymers can be achieved in a variety of ways, described in detailed reviews on alignment strategies and related device opportunities.<sup>25–29</sup> This section provides a concise overview of various alignment approaches, ranging from solution-guided methods to solid-state manipulation. In [Figure 2](#), we highlight the most prevalent alignment techniques for conjugated polymer films, displaying the *DR* attained by each method for single-material thin films. Each technique can achieve a high degree of in-plane alignment depending on the material and processing conditions. While strain alignment has not traditionally yielded the highest *DR*s, recent demonstrations have pushed the boundary of strain alignment to achieve *DR*s of nearly 40.<sup>30</sup> It is worth noting that Hamidi-Sakr et al. employed high-temperature rubbing of doped P3HT resulting in a *DR* exceeding 50.<sup>31</sup> However, this was facilitated by the addition of the dopant  $\text{F}_4\text{TCNQ}^-$  and therefore not included in [Figure 2](#). Additionally, there are several less commonly used alignment strategies, including film compression, melt-drawing, photoalignment, electric/magnetic field alignment, and roll transfer, which are not depicted in [Figure 2](#). A summary of alignment demonstrations can be found in [Table S1](#).

### Solution assembly

A broad range of methods fall under the category of solution-based alignment, typically involving the manipulation of the meniscus flow of the solution, use of shear forces on the solution, or guided epitaxial assembly. Meniscus-guided coating is an approach that relies on controlled motion of the solution meniscus through viscous drag enacted by gravity or a coating head. There are two schemes based on the coating speed: (1) lower speed capillary regime and (2) higher speed Landau-Levich regime.<sup>33</sup> In the lower speed regime, the interplay of capillary forces

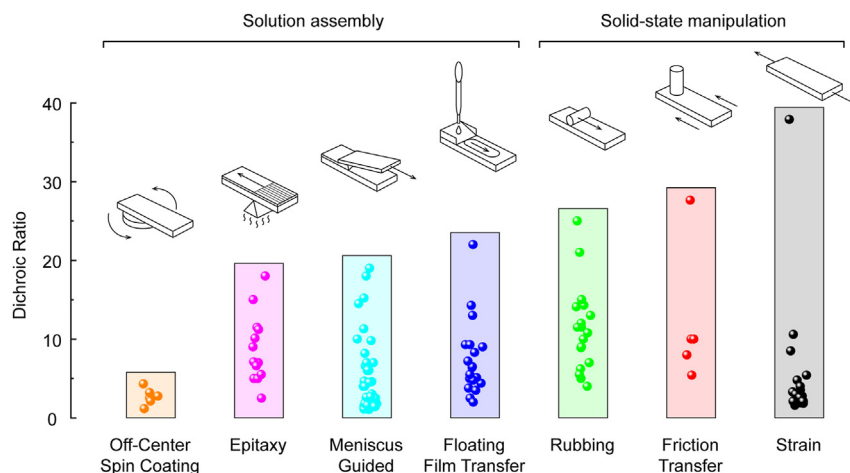


**Figure 2. Optical dichroic ratio of aligned conjugated polymer thin films**

Alignment techniques include popular solution assembly and solid-state manipulation methods. These strategies include off-center spin coating, epitaxy, meniscus-guided coating, floating film transfer, rubbing, friction transfer, and strain. Details and references can be found in [Table S1](#).

with solvent evaporation typically leads to polymer backbone alignment perpendicular to the coating direction. The higher speed regime relies primarily on the shear forces acting on the film, inducing a polymer backbone alignment parallel to the coating direction. However, the final in-plane orientation of the backbone is influenced by additional factors beyond coating speed, including solution concentration and the presence and structure of aggregates in solution.<sup>34–36</sup> This approach can be modified through utilizing various coating blade designs.<sup>37,38</sup> Off-center spin coating utilizes a high centrifugal force applied to a polymer solution by placing a substrate away from the center of rotation.<sup>39,40</sup> Solution-based epitaxy methods drive polymer assembly guided from solution by a geometric or electrostatic feature of the substrate or a second solidifying component in the solution. Epitaxial alignment has been achieved using templating on rubbed polymer substrates,<sup>41,42</sup> nano-grooved substrates,<sup>43,44</sup> or using crystallizing aromatic solvents.<sup>45,46</sup> Lastly, the solidification can be manipulated while on a hydrophilic liquid substrate, referred to as the floating film transfer method.<sup>47</sup> In this approach, the hydrophilic substrate results in a compressive force and interfacial friction when casting the polymer solution of interest, allowing for the expansion of the film and macroscopic alignment.

### Solid-state manipulation

Mechanical methods to orient films in the solid state include rubbing, friction transfer, and strain. In rubbing, a microfiber or velvet cloth is typically used, and heat is often applied to improve molecular mobility. A schematic of high-temperature rubbing and the corresponding polarized ultraviolet-visible (UV-vis) absorbance spectra for several materials can be seen in [Figures 3A and 3B](#).<sup>48</sup> Rubbing was initially utilized in the large-scale orientation of liquid crystals in LCDs,<sup>49–51</sup> but is also highly effective for conjugated polymers.<sup>48,52–54</sup> During high-temperature rubbing, the cloth fibers apply a shear force on the polymer chains, resulting in preferential alignment of the relatively stiff polymer backbone in the direction of rubbing. Elevating the sample's temperature during rubbing leads to the partial melting of polymer side chains, facilitating the disentanglement of polymer chains.<sup>48</sup> The utilization of lower molecular weight polymers can also enhance polymer alignment by reducing polymer entanglements.<sup>48,55</sup> Friction transfer has also proven to be an effective

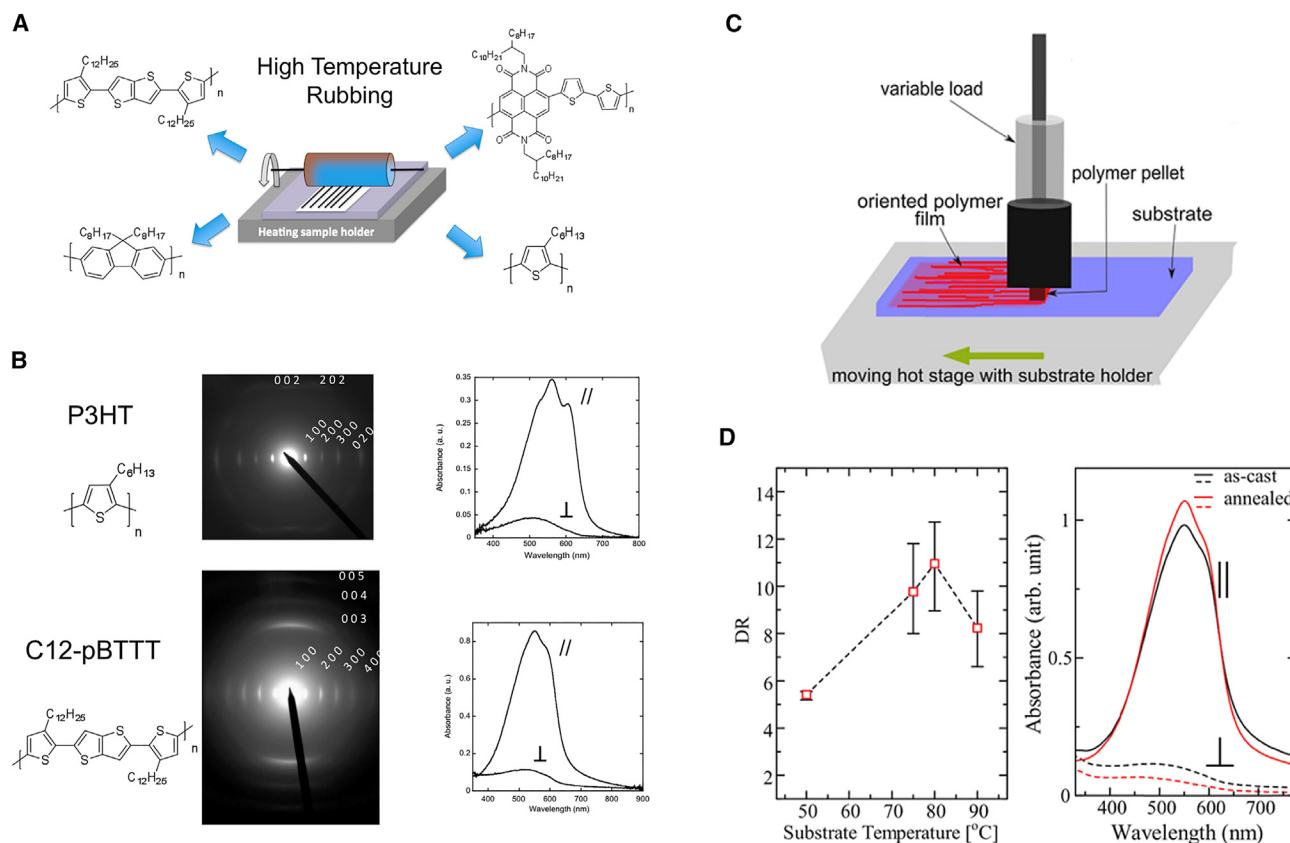


**Figure 3. Solid-state manipulation alignment strategies**

(A and B) Schematic of high-temperature rubbing (A),<sup>48</sup> along with (B) electron diffraction and polarized UV-vis absorbance spectra for P3HT and C12-pBTTT films aligned using high-temperature rubbing. Reproduced with permission.<sup>48</sup> Copyright 2014, American Chemical Society. (C and D) Schematic of friction transfer processing (C),<sup>61</sup> along with (D) dichroic ratio versus substrate temperature and polarized UV-vis absorbance spectra for PBTBT aligned using friction transfer. Reproduced with permission.<sup>61</sup> Copyright 2020, American Chemical Society.

mechanical alignment technique. This method employs a solid polymer block, transferring a thin layer through a drawing process onto a heated substrate. A schematic for the process and polarized absorbance spectra is depicted in Figures 3C and 3D. The shearing forces in friction transfer have been identified as the driving force behind polymer alignment. Friction transfer has been utilized to induce anisotropic electroluminescence in thin films<sup>56–58</sup> and to create a template substrate for the oriented growth of materials.<sup>44,59,60</sup>

#### Strain alignment method

Strain alignment of conjugated polymer films is typically conducted while they are laminated on an elastomer support, as illustrated in Figure 4. The process involves either directly casting a polymer film onto the elastomer or transferring it from a donor substrate onto the elastomer. Strain is then imparted on the film-elastomer composite. While under strain, the film is transferred from the elastomer support to a final receiving substrate. This transfer process relies on a cascading differential adhesion between each transfer interaction. The adhesion between the film/stamp must be greater than the film/donor to pick up the film, and adhesion between the film/receiver must be greater than the film/stamp when printing the film.<sup>62</sup> PDMS is often the preferred elastomer for this application due to its smooth, non-reactive surface with relatively weak adhesion with the polymer semiconductor.<sup>1,18</sup> However, when the cascading adhesion sequence is not met, various approaches

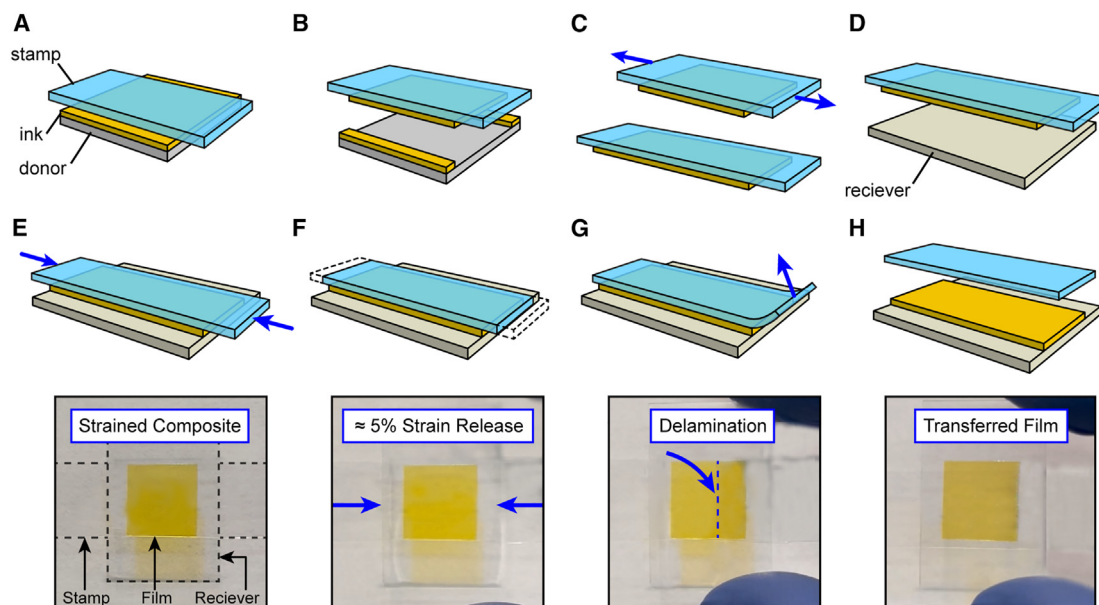


**Figure 4. Illustration of the SHARP transfer printing method**

(A) Lamination of the elastomer stamp onto the film, (B) transfer of the film to the stamp, (C) strain applied to the film/elastomer composite, (D) the film laminated onto the receiving substrate, (E and F) strain reduced by  $\sim 5\%$ , (G) normal force applied to leading edge of the stamp to delaminate the film, and (H) removal of the stamp. Bottom row includes pictures corresponding to steps (E) through (F).

have been developed to overcome this limitation.<sup>1,62–67</sup> One approach is to cast a sacrificial layer between the thin film and the donor substrate.<sup>64</sup> After the elastomer is laminated onto the polymer, the sacrificial layer is removed, usually by selectively dissolving the sacrificial layer, to delaminate the film from the donor substrate. In the printing step, if the adhesion criterion is not met, surface treatments of the receiving substrate have been employed. These treatments include  $O_2$  plasma, UV-ozone, or adding an adhesive layer (e.g., sucrose<sup>68</sup>). However, these strategies may have adverse effects on the quality of the printed film or underlying layer, potentially impacting device performance.<sup>69</sup> Alternatively, one can increase the rate of stamp removal, exploiting the viscoelastic nature of the PDMS to modify its adhesive properties.<sup>70</sup> In addition, Sen et al. have outlined a printing strategy called SHARP (shear-assisted organic printing), illustrated in Figure 4.<sup>67</sup> In the SHARP approach, once the strained film is in contact with the receiving substrate, the nominal strain applied to the PDMS-film composite is released slightly ( $\approx 5\%$ ) resulting in a shear load across the film. This shear load then imparts a bending moment at the leading edge of the stamp, promoting film delamination.<sup>67</sup> As the stamp is removed, the shear load at the stamp/film leading edge ensures continuous film transfer from the stamp to the receiving substrate. This method has been used to print films onto a variety of substrates including glass, silicon, polyethylene terephthalate (PET), and even low-surface-energy octyltrichlorosilane (OTS)-treated silicon.<sup>67,71,72</sup> Moreover, this process has been used in device fabrication including OFETs and OPDs.<sup>55,72–74</sup>

### Thermomechanical considerations

In this section, we consider the mechanical measurements to probe film behavior under uniaxial strain and the central factors that impact the ductility of conjugated polymer thin films. For more extensive reviews on design strategies to achieve ductile films for stretchable electronics, we refer the reader to other reviews.<sup>23,24,75–77</sup>

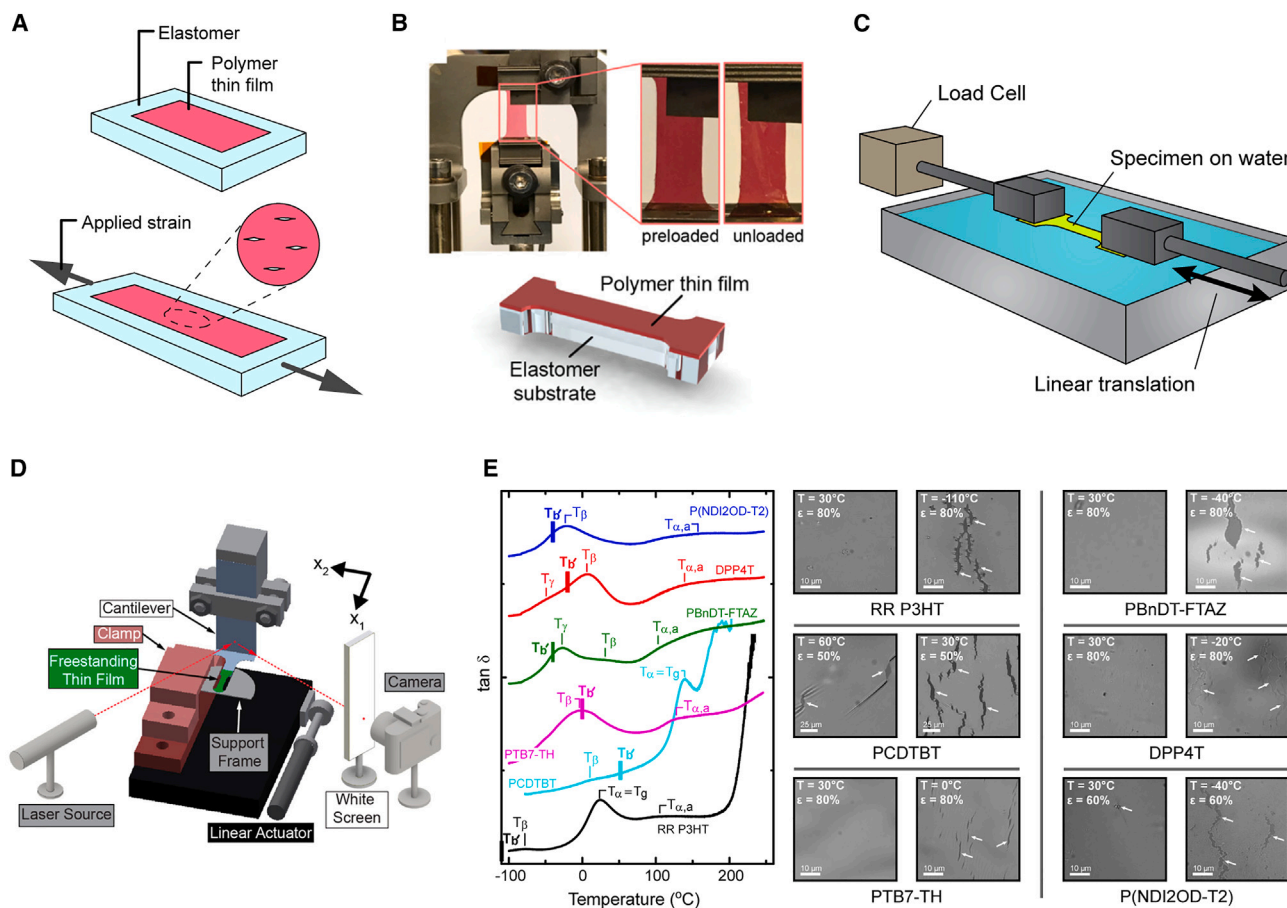


**Figure 5. Tensile strain mechanical measurements**

(A) Film on elastomer (FOE) crack onset strain (COS).

(B) Film laminated on thin elastomer (FLOTE). Reproduced with permission.<sup>85</sup> Copyright 2020, American Chemical Society.

(C) Film on water (FOW).

(D) Tensile tester for ultrathin freestanding film (TUFF). Reproduced with permission.<sup>92</sup> Copyright 2019, American Chemical Society.

(E)  $\tan \delta$  curves of different polymers from DMA temperature sweeps, with observed thermal transitions and the toughness transition ( $T_{\beta}$ ) labeled. To the right are microscope images at 30°C and at the respective  $T_{\beta}$  at the specified strains. The films were strained along the horizontal axis of the page. Reproduced with permission.<sup>96</sup> Copyright 2020, American Chemical Society.

### Mechanical characterization methods

For successful strain alignment, the polymer film must be ductile enough to undergo substantial tensile strain without fracturing. Consequently, assessing film ductility is critical to determine its suitability for strain alignment. In addition to ductility, it is valuable to understand the complete stress-strain behavior of the film under tension. This provides additional property information including Young's modulus, yield stress, and strain hardening that informs the mechanical response of the film when strained on an elastomer support or in a device. The simplest and most direct method to assess the film ductility is to strain the film while on an elastomer support until cracks are observed in the film, termed crack onset strain (COS) and illustrated in Figure 5A.<sup>78–82</sup> The manipulation of the film while on an elastomer (or film on elastomer [FOE]) can be further extended to provide various mechanical characteristics including Young's modulus, yield strain, stress-relaxation behavior, and toughness.<sup>81–84</sup> However, the stress-strain behavior of polymer thin films cannot be quantitatively captured when using bulk elastomer substrates. To address this limitation, an ultrathin elastomer support with thickness of less than 5  $\mu\text{m}$  can be employed.

This reduces the stiffness of the substrate so that the mechanical properties of the conjugated polymer can be observed through tensile testing, as depicted in Figure 5B.<sup>85</sup> Additionally, the composite structure enables an examination of the influence of the substrate on film ductility. The support also allows for tensile tests using a temperature-controlled environment to capture viscoelastic film behavior.<sup>85</sup> To remove the effect of neighboring substrates on film mechanical behavior, pseudo-freestanding and completely freestanding tensile tests have been developed. Given the thinness of the polymers of interest (<300 nm), it is difficult to test freestanding films. To overcome this limitation, tensile tests can be performed by floating the thin film of interest on the surface of water, coined film on water (FOW) (Figure 5C).<sup>86–91</sup> While FOW tests capture stress-strain thin film characteristics, they have a limited temperature range and the potential for film swelling due to water contact.<sup>89,92</sup> To expand the temperature range, ionic liquids have been introduced as a floating medium in a technique called film-on-ionic liquid.<sup>93</sup> More recently, tensile tests on completely freestanding thin films have been demonstrated, eliminating any external influence on the behavior of a film, with an example illustrated in Figure 5D.<sup>92,94,95</sup> While this method provides stress-strain behavior free of substrate influence, handling the films remains a challenge.

Plastic deformation in polymer films requires molecular rearrangements in the amorphous or crystalline domains.<sup>97</sup> Capturing thermal transitions in the polymer, especially within the amorphous component, establishes the temperature at which various molecular features become mobile and can undergo conformational changes.<sup>95,97</sup> Dynamic mechanical analysis (DMA) stands out as a highly sensitive tool to measure thermal transitions in polymers.<sup>98,99</sup> While thermal analysis techniques such as differential scanning calorimetry are commonly used to measure thermal transitions in polymers, there are often low enthalpic and heat capacity changes across thermal transitions in conjugated polymers resulting in weak signals.<sup>100,101</sup> Some conjugated polymers, such as P3HT, exhibit a well-defined glass transition temperature ( $T_g$ ), but defining a  $T_g$  in conjugated polymers can be difficult, particularly donor-acceptor (DA) type polymers.<sup>100</sup> Yet, the sensitivity of DMA has revealed complex thermal relaxation characteristics in DA polymers, where the most prominent relaxation is attributed to side-chain dynamics.<sup>96,98,99</sup> The phase behavior is also complicated by the crystal types the polymers can adopt, including paracrystallinity and liquid crystallinity.<sup>102,103</sup> In polymers, the relaxation below its  $T_g$  (i.e., secondary or  $\beta$ -transition) is often called the toughness transition because the film ductility can drop significantly when it is below this transition temperature.<sup>96</sup> Indeed, it has been shown that the ductility and toughness of a number of polymer semiconductors were reduced when they were strained below their side-chain relaxation temperature ( $T_\beta$ ), displayed in Figure 5E.<sup>96</sup> These observations are consistent with other reports that have highlighted the role of side chains on the ductility of the semiconducting polymers.<sup>104</sup> It should be noted that while ductility is correlated to thermal transitions of conjugated polymers, it can still vary significantly both above and below these relaxations. For example, below the  $\beta$ -transition, conjugated polymers may continue to allow for deformation possibly through active slip systems in crystals.<sup>96</sup>

### Molecular structure

The plasticity of a film is intricately tied to the polymer structure. Key factors, including molecular weight and the chemistry of both the backbone and side chains dictate the film's ultimate strain limit and its achievable degree of alignment. Beyond alignment, the molecular features driving plasticity are important for successful implementation of polymers in stretchable electronics, and we refer the reader to other

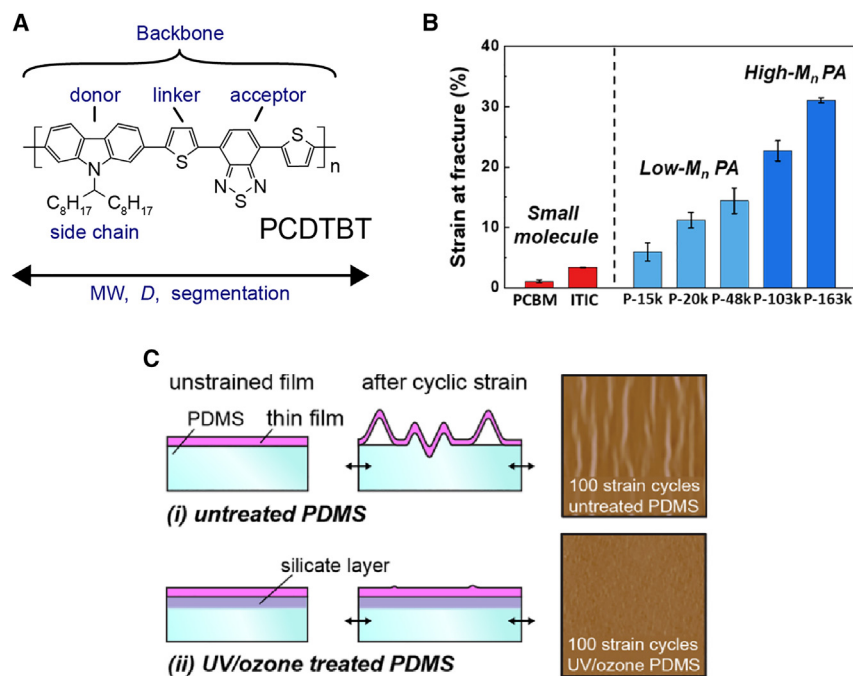


**Figure 6. Molecular considerations of straining polymer semiconductors**

(A) Schematic of the principal molecular features that dictate the mechanical properties of conjugated polymer film.

(B) Ductility of blend films with varying acceptors including small molecules and low/high molecular weight polymer P(NDI2OD-T2). Reproduced with permission.<sup>117</sup> Copyright 2019, American Chemical Society.

(C) Effect of surface UV/ozone treatment on elastomer substrate for buckling/delamination of a thin polymer film. Reproduced with permission.<sup>69</sup> Copyright 2019, American Chemical Society.

excellent reviews covering that application.<sup>76,97,105–109</sup> While predicting plasticity based on molecular structure is not currently possible, there are several factors that are recognized to be important, as summarized in Figure 6A. To achieve ductile films, one of the primary considerations is to have sufficiently high molecular weight (MW).<sup>104,110–114</sup> The role of MW on film ductility has been demonstrated in various polymer semiconductors including P3HT,<sup>112,114,115</sup> PBnDT-FTAZ,<sup>116</sup> and P(NDI2OD-T2) (Figure 6B).<sup>117,118</sup> The increase in ductility typically found with increasing MW is generally attributed to two main factors: (1) the formation of polymer entanglements in the amorphous domains, which increases intermolecular coupling, and (2) an increase in the formation of molecular tie chains between ordered crystals or aggregates. Both effects increase the distribution of stress around a defect and reduce the occurrence of failure through chain pullout. High MW is also critical in polymer blend films, where higher MW of both polymers supports ductility. Having only one polymer with high MW can still improve ductility of the blend; however, the influence of MW on ductility depends on the material systems and range of molecular weights considered.<sup>117,119</sup>

When considering the monomer structure, both the side-chain and backbone structures can influence ductility. In most conjugated polymers, the side chains are disordered and weakly interacting, primary serving to enhance solubility. However, their chemical structure, size, and placement can impact mechanical behavior.<sup>120–124</sup> For instance, Savagatrup et al. conducted a study on the mechanical properties of poly(3-alkylthiophenes) through varying the length of the alkyl side chains.<sup>120</sup> As

the side-chain length increased, there was a general increase in the COS and a decrease in elastic modulus. This change was attributed to a reduction in the volume fraction of load-bearing main-chain bonds.<sup>120</sup> Longer side-chain lengths have also been found to reduce the  $T_g$  of the polymer.<sup>107,124</sup> Additionally, introducing segmental variation by modifying the backbone or side chains has also been shown to modify film mechanical properties.<sup>24,125,126</sup> The regioregularity of conjugated polymers may also affect mechanical characteristics. While increasing regioregularity is often desired to improve charge mobility, it can have an adverse effect on ductility. In the case of P3HT, a decrease in regioregularity has been demonstrated to lower crystallinity and increase ductility.<sup>126</sup>

Recently developed high-performance semiconducting polymers have been designed by incorporating alternating DA moieties. These polymers commonly feature fused aromatic ring structures, resulting in extended persistence lengths and increased rigidity. More generally, polymer structures with fused rings tend to be stiffer and more brittle when compared with those with rings bonded through single c–c bonds.<sup>83,106,127</sup> For example, Lu et al. demonstrated the impact of introducing a thiophene spacer in the backbone of poly(tetrathienoacene-diketopyrrolopyrrole)-based polymers. This modification led to a lower modulus and higher COS compared to the polymer without the spacer.<sup>127</sup> Conjugation break spacers have also been used to improve the stretchability and processability of polymer semiconductors.<sup>128</sup> These non-conjugated flexible spacers have been shown to improve plasticity of polymer films with limited hinderance on electrical performance. Although, their mechanical properties remain dependent on additional factors such as the packing structure.<sup>129</sup> Oh et al. explored the effect of conjugated break spacers with varying structures for flexible and healable thin-film organic transistors.<sup>130</sup> The addition of these spacers facilitated the creation of non-covalent cross-linking sites through hydrogen bonding. This contributed to the dissipation of energy under tensile loading, improving the stretchability of the polymer films. The authors also observed healing of the fractured film following solvent and thermal treatment. Ductility can also be related to the morphology of a film, especially as it relates to aggregation and crystallinity.<sup>131</sup> While long-range order may improve the charge mobility of the polymer semiconductor, there have been reports that it can come at the cost of ductility.<sup>131</sup>

### Neighboring substrate

The COS of a polymer film can be enhanced when straining it on an elastomer substrate, as compared to a freestanding film.<sup>132</sup> On an elastomer, the stress can be redistributed throughout the film, alleviating stress concentrations and negating a necking instability.<sup>78</sup> Utilizing an elastomer with modulus closer to the modulus of the film will reduce interfacial stresses, increasing the COS and hence the ultimate polymer alignment that can be achieved in strained polymer films.<sup>80,133</sup> The elastic characteristics of a bilayer structure can be described by the Dundur parameters,<sup>80,134</sup>

$$\alpha = (\bar{E}_f - \bar{E}_s) / (\bar{E}_f + \bar{E}_s), \quad (\text{Equation 1})$$

$$\beta = \frac{1}{2} \frac{\mu_f(1 - 2\nu_s) - \mu_s(1 - 2\nu_f)}{\mu_f(1 - \nu_s) + \mu_s(1 - \nu_f)}. \quad (\text{Equation 2})$$

Here,  $\bar{E} = E/(1 - \nu^2)$ ,  $\mu = E/(2(1 + \nu))$ ,  $\nu$  is the Poisson ratio, and subscripts “f” and “s” refer to the film and substrate, respectively. As parameter  $\alpha$  approaches 1 ( $E_f \gg E_s$ ), the likelihood of a crack forming and propagating in a film under strain increases. This is due to an increase in the strain energy release rate ( $G$ ) caused by the

concentration of stress at the film-substrate interface.<sup>80,135</sup> Fracture occurs when  $G$  exceeds the critical value known as the cohesive fracture energy ( $G_c$ ).<sup>136</sup> The elastomer substrate can be modified to help overcome the elastic mismatch in the bilayer system. Using a higher cross-linker density in the elastomer leads to a stiffer substrate, lowering the modulus difference between the elastomer and thin film. A disadvantage to this approach is that a stiffer elastomer will often have a lower rupture strain, limiting the extent the film can be strained. An alternative method is to increase the surface energy and stiffness of the elastomer substrate through UV-ozone treatment.<sup>69,137,138</sup> The increase in surface energy promotes adhesion on the film to the elastomer, assisting the distribution of stress throughout the film, and the modulus mismatch reduces at the film-elastomer interface (Dundur parameter  $\alpha \rightarrow 0$ ). Sun et al. demonstrated this approach to achieve stretchable diketopyrrolopyrrole-type polymer (PDPP-4T) films.<sup>69</sup> Using UV-ozone-treated PDMS during cyclic straining of PDPP-4T greatly reduced wrinkling and delamination (seen in Figure 6C), demonstrating the importance of tuning the substrate-film interface in stretchable polymers. Furthermore, confining a polymer fibril in an elastomer matrix has been demonstrated to greatly enhance the COS of a polymer.<sup>139</sup> Xu et al. demonstrated that nanoscale fibrils of a conjugated polymer resulted in nanoconfinement effects that enabled biaxial stretchability of the composite of up to 100% without fracture or drop in electrical performance.<sup>139</sup> Solid additives, often in the form of small molecule plasticizers or elastomers, also have an effect on the ductility and  $DR$  of a polymer semiconductor film. They generally increase the film plasticity and ductility, depending on additive loading, MW, and segregation.<sup>119,140</sup>

### Morphological characterization of aligned films

Many of the same tools used to characterize organic electronic film morphology are applicable when applied to aligned films.<sup>141,142</sup> In-plane anisotropy can add information about microstructure of the polymers but can also complicate the interpretation of common characterization methods. This section reviews the most widely used characterization tools for probing the morphology of aligned films and discusses the challenges associated with analyzing oriented films. Specifically, the tools under consideration are illustrated in Figure 7 and include UV-vis spectroscopy, spectroscopic ellipsometry, X-ray scattering, atomic force microscopy (AFM), and transmission electron microscopy (TEM).

#### UV-Vis spectroscopy

Polarized UV-vis spectroscopy has been widely used to quantitatively determine the degree of backbone alignment. The absorbance of light is proportional to  $\langle (\vec{E} \cdot \vec{M})^2 \rangle$ , where  $\vec{E}$  is the electric field of the light, and  $\vec{M}$  is the optical transition dipole moment of the polymer. Density functional theory modeling has shown that as the degree of polymerization increases beyond several monomers, the  $\pi$ - $\pi^*$  transition dipole aligns along the polymer backbone.<sup>143</sup> This alignment has been attributed to the intramolecular coupling of atomic orbitals. Thus, absorbance is maximized when  $\vec{E}$  is parallel to the polymer backbone and goes to zero if orthogonal. To measure the net in-plane orientation of the polymer, polarized light is rotated to capture the angular dependence of the film absorbance, as illustrated in Figure 7. The polarized light orientation that results in maximum absorbance then corresponds to the direction of polymer alignment. In conjugated polymers, the polymer chains usually orient in the direction of strain, and thus polarized light absorbance is maximized when the polarization is parallel to the strain direction. The degree of alignment is most often captured by the  $DR$ , which is the ratio between these extremes of absorbance described by  $A_{\parallel}(\lambda)/A_{\perp}(\lambda)$ , where  $A_{\parallel}$  and  $A_{\perp}$  are the absorbance with incident polarized light oriented parallel ( $0^\circ$ ) and perpendicular ( $90^\circ$ ) to the director (stretch

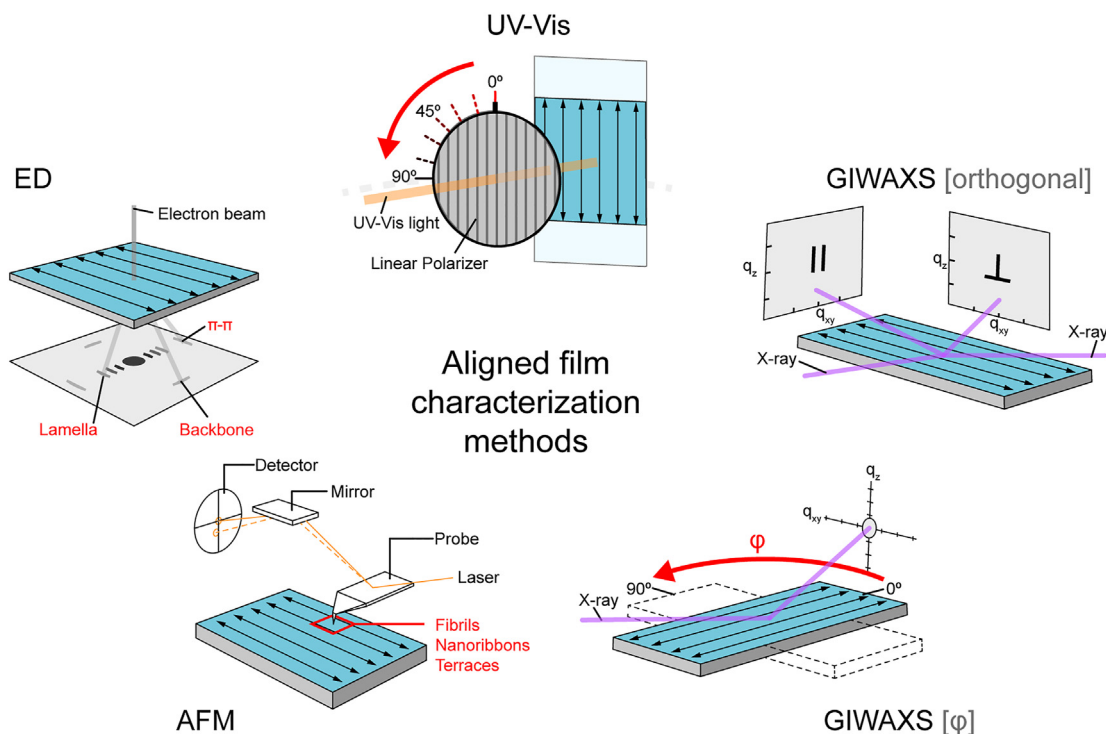


**Figure 7. Common tools to characterize aligned films**

Includes polarized ultraviolet-visible (UV-vis) spectroscopy, grazing incidence wide-angle X-ray scattering (GIWAXS) with orthogonal film orientations (parallel and perpendicular), GIWAXS with in-plane  $\phi$  rotation, atomic force microscopy (AFM), and electron diffraction (ED).

direction), respectively. An example can be seen in Figures 8A and 8B, where the polarized absorbance and dichroic ratio for a blend film of PBnDT-FTAZ:P (NDI2OD-T2) at different extents of strain is displayed. The anisotropy can also be captured by the linear dichroism ( $LD$ , represented as  $A_{\parallel}(\lambda) - A_{\perp}(\lambda)$ ) or diattenuation ( $(T_{\max} - T_{\min}) / (T_{\max} + T_{\min})$ , where  $T_{\max}$  and  $T_{\min}$  represent the maximum and minimum transmitted light intensities through a sample).  $LD$  and diattenuation are less prevalent than  $DR$  in the field of organic electronics compared to their use in biosciences and optics.<sup>144,145</sup>

An order parameter can be used to quantify the degree of alignment from the measured  $DR$ . This is often used to characterize alignment in liquid crystals.<sup>103</sup> The order parameter can be given in either 2D or 3D space. For polymer thin films, assuming the polymer chains are lying predominately in the plane of the films, a 2D order parameter can be applied to assess the degree of uniaxial in-plane alignment. The 2D order parameter is given by

$$S_{2D} = 2\langle \cos^2 \phi \rangle - 1, \quad (\text{Equation 3})$$

where  $\phi$  is the angle between the element (backbone) and director (stretch direction), with the brackets representing an ensemble average over the identified population.  $DR$  can also be used to compute  $S_{2D}$ . Given that  $A_{\parallel}$  and  $A_{\perp}$  are proportional to  $\langle \cos^2(\phi) \rangle$  and  $(1 - \langle \cos^2(\phi) \rangle)$ ,  $DR$  can be written as

$$DR = \frac{\langle \cos^2(\phi) \rangle}{(1 - \langle \cos^2(\phi) \rangle)}. \quad (\text{Equation 4})$$

Rearranging leads to

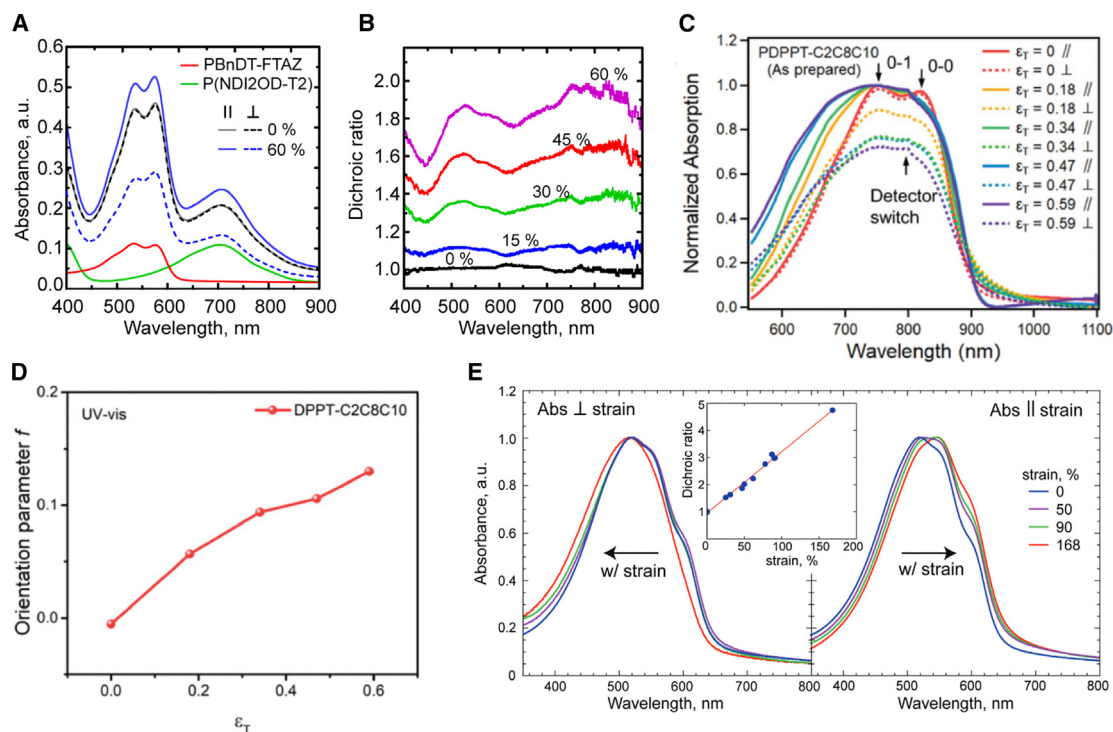


**Figure 8. UV-vis spectroscopy characterization of aligned polymer semiconductor films**

(A and B) Polarized UV-vis absorbance spectra (A) of PBnDT-FTAZ:P(NDI2OD-T2) blend films strained 0% and 60% and (B) corresponding spectral DR of strained PBnDT-FTAZ:P(NDI2OD-T2) films. Reproduced with permission.<sup>74</sup> Copyright 2018, John Wiley and Sons.

(C and D) Polarized UV-vis absorbance spectra (C) for PDPPT-C2C8C10 films under various strains and (D) orientation parameter ( $f$ ) of strained PDPPT-C2C8C10 films, labeled as  $S_{2D}$  in this review. Reproduced with permission.<sup>123</sup> Copyright 2021, John Wiley and Sons.

(E) Normalized absorbance of P3HT films under varying levels of strain with light polarized perpendicular (left) and parallel (right) to the strain direction. Reproduced with permission.<sup>1</sup> Copyright 2011, John Wiley and Sons.

$$\langle \cos^2(\phi) \rangle = \frac{DR}{DR+1}. \quad (\text{Equation 5})$$

Inserting this relation into the 2D order parameter gives

$$S_{2D} = \frac{DR - 1}{DR+1}. \quad (\text{Equation 6})$$

An example of  $S_{2D}$  can be seen in Figures 8C and 8D, showing strain-dependent polarized absorbance and  $S_{2D}$  of a PDPPT-C2C8C10 film.<sup>123</sup>

The DR is most often reported at a single wavelength, frequently at the peak absorption wavelength for the material. However, this can be misleading, as DR is not constant across the spectrum. Part of the difficulty lies in the spectral shift that is often seen when aligning semiconducting polymer films. Absorbance spectra with light polarized parallel to the straining direction can be red shifted, with a corresponding blue shift under perpendicularly polarized light. This is frequently associated with an increase in the resolution of certain vibronic features (e.g.,  $0 \rightarrow 0$  transition) seen under parallel polarized light. These changes in the polarized UV-vis spectra indicate an increase in local order for the polymers aligned in the direction of strain, or that the more ordered material re-orientes more fully in the direction of strain.<sup>1,146</sup> For example, a spectral shift was observed in strain-aligned P3HT, with a red shift and increase in the  $0 \rightarrow 0$  transition under parallel polarized light and subsequent blue shift and loss of vibronic feature under perpendicular polarized light

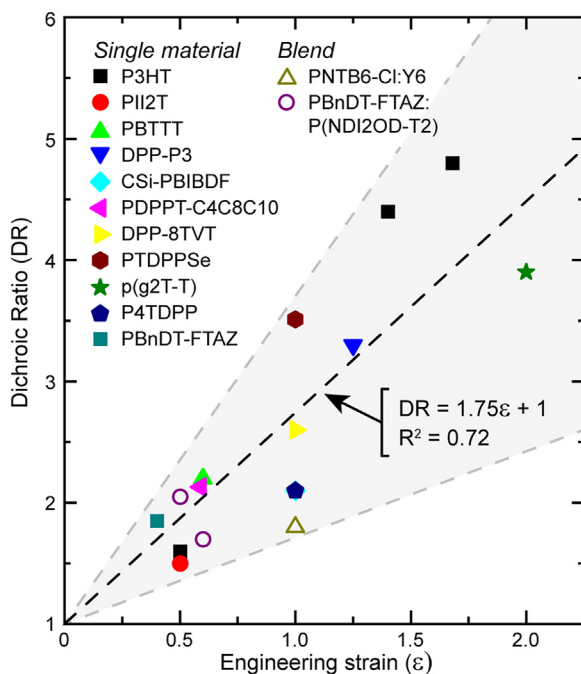


**Figure 9. Dichroic ratio vs. engineering strain for polymer semiconductors**

Includes a variety of single-material (closed symbols) and blend (open symbols) films without post-strain treatment. All films were strained on an elastomer support. A summary table can be found in [Table S2](#).

(Figure 8E).<sup>1</sup> This was attributed to preferential reorientation of the crystalline versus amorphous material during straining. Given the difficulty in fully describing the orientation distribution function on the polymer in an aligned film, reporting *DR* at the peak absorption wavelength in the parallel direction is a reproducible figure of merit that can be used to quantify a 2D order parameter.

It is important to note that the relationship between strain and degree of alignment captured through the *DR* depends on the polymer structure and film morphology. [Figure 9](#) depicts the *DR* versus strain for various neat and blend polymer films. While there is a general positive trend between strain and alignment, there remains a range of *DR* values found for a given strain depending on the polymer. Further research is needed to establish what factors dictate this relationship.

### Spectroscopic ellipsometry

Spectroscopic ellipsometry (SE) examines aligned films by capturing the biaxial dielectric function ( $\epsilon_{xx} \neq \epsilon_{yy} \neq \epsilon_{zz}$ ). Once the dielectric function is known, the anisotropic extinction coefficient (*k*) can be determined. SE is akin to UV-vis spectroscopy since the absorption coefficient ( $\alpha$ ) is directly related to *k* by  $\alpha = \frac{(4\pi k)}{\lambda}$ . However, SE offers several advantages over polarized UV-vis spectroscopy. First, it provides additional polymer orientation information, including out-of-plane orientation of the polymer backbone. In UV-vis spectroscopy, issues related to scattering and surface reflections can introduce uncertainties into absorbance measurements. Additionally, a transparent or semitransparent substrate must be used in UV-vis spectroscopy, which may not match the substrate employed in final applications. SE bypasses these limitations by detecting changes in the polarization states of a light source upon interaction with the sample. In addition, by probing the sample at varying angles of illumination and detection, out-of-plane optical constants can be

determined, and vertical changes in optical properties can be modeled. In the case of aligned films, the variation in optical properties through the film thickness can provide insight into changes in the degree of in-plane alignment through the film.

Films with anisotropic optical properties require careful ellipsometry analysis. The optical response of a material can be described by the complex, frequency-dependent, dielectric function, given as<sup>147</sup>

$$\epsilon_{ij} = \begin{bmatrix} \epsilon'_{xx} + i\epsilon''_{xx} & 0 & 0 \\ 0 & \epsilon'_{yy} + i\epsilon''_{yy} & 0 \\ 0 & 0 & \epsilon'_{zz} + i\epsilon''_{zz} \end{bmatrix}. \quad (\text{Equation 7})$$

The observed dielectric tensor arises from the spatially averaged local polarization that is a function of the local dielectric function and the orientation distribution function(s) describing the material. The measured dielectric function arises from the local dielectric response of the polymer and the orientation distribution function of the polymer that makes up the film. Assuming the absorption dipole is oriented parallel to the polymer backbone (c-axis) and has cylindrical symmetry, the local dielectric tensor can be given as<sup>147</sup>

$$\begin{bmatrix} \epsilon'_{aa} & 0 & 0 \\ 0 & \epsilon'_{aa} & 0 \\ 0 & 0 & \epsilon'_{cc} + i\epsilon''_{cc} \end{bmatrix}. \quad (\text{Equation 8})$$

Taking this local dielectric tensor, and using a linear effective medium approximation, the imaginary part of the orthorhombic dielectric function is given as<sup>147</sup>

$$\begin{bmatrix} \frac{1}{2} \langle \sin^2 \theta \sin^2 \phi \rangle & 0 & 0 \\ 0 & \frac{1}{2} \langle \sin^2 \theta \cos^2 \phi \rangle & 0 \\ 0 & 0 & \cos^2 \theta \end{bmatrix} \epsilon''_{cc}, \quad (\text{Equation 9})$$

where the Euler angles  $\psi$ ,  $\theta$ , and  $\phi$  orient the local a, b, c frame in the orthorhombic and x, y, z frame. To quantify the degree of backbone alignment in the plane of the film, a 2D order parameter can be calculated using the imaginary components of the x ( $\epsilon''_{xx}$ ) and y ( $\epsilon''_{yy}$ ) dielectric tensor, given as<sup>147</sup>

$$S_{2D} = 2 \langle \cos^2(\phi) \rangle - 1 = \frac{\epsilon''_{yy} - \epsilon''_{xx}}{\epsilon''_{xx} + \epsilon''_{yy}}. \quad (\text{Equation 10})$$

SE is highly accurate and robust as it measures the complex ratio of a particular system rather than absolute values. However, the generated results of ellipsometry require models to unveil the underlying optical properties of a film. When measuring thin conjugated polymer films, the projection of the electric field absorption in the z-direction (out of plane) is very small. This limited sensitivity can result in strong correlations in the fit parameters for out-of-plane optical constants. These limitations can be addressed by using multiple angles of incidence and measuring several films with varying thicknesses or on different substrates. By employing a robust experimental procedure and model construction, an accurate depiction of the biaxial dielectric components can be obtained to capture film anisotropy.

### X-ray scattering

Alongside UV-vis spectroscopy, the most common measurements to capture the anisotropic microstructure of aligned organic electronic films are X-ray scattering

techniques. There are multiple reviews that cover X-ray scattering measurements of conjugated polymers.<sup>141,148</sup> Here, we discuss the X-ray scattering techniques applied to aligned films, along with associated challenges specific to capturing in-plane anisotropy. The predominant technique used is grazing incidence wide-angle X-ray scattering (GIWAXS), typically conducted in a synchrotron facility where the grazing incidence and high flux is able to capture molecular packing from the thin films that are often poorly ordered. The diffraction of X-rays is determined by the spacing and orientations of crystallographic planes of the film determined through Bragg's law. GIWAXS measurements often employ area detectors, which allow for rapid collection of a range of scattering angles at the expense of resolution. The resulting peaks represent the magnitude and direction of the reciprocal lattice vectors of crystals in the film, which are related to the interplanar spacing. When analyzing anisotropic films, it's common to measure the scattering with the X-ray source parallel and perpendicular to the alignment direction. A schematic for probing anisotropic films using GIWAXS is given in Figure 7. As the polymer chains orient in the direction of strain, the scattering associated with backbone ordering (00l) will strengthen for the X-ray beam perpendicular to the strain direction, and in-plane (h00) and (0k0) scattering will strengthen for the X-ray beam parallel to the strain direction (assuming face-on and edge-on stacking are present). However, a direct comparison of the 2D images can be misleading, as the X-ray flux may vary for each measurement, and the sample volume being probed may differ. To compare the parallel and perpendicular scattering intensities, the data can be normalized by the out-of-plane scattering intensity. The out-of-plane scattering along  $Q_{xy} = 0$  should ideally be independent of the incident beam direction. However, specular diffraction along  $Q_z$  with  $Q_{xy} = 0$  is not observed due to the projection of the probed reciprocal space (Ewald sphere surface) onto a flat plate.<sup>149</sup> Nevertheless, normalizing near out-of-plane scattering provides a path to more accurate estimate of anisotropic packing. In films with in-plane alignment, a similar problem occurs. In the case of parallel planes oriented along the alignment direction, the in-plane data  $Q_{xy}$  with  $Q_z = 0$  may not represent specular scattering.<sup>141</sup>

Furthermore, capturing scattering from orthogonal X-ray beams provides an incomplete set of data necessary to determine a change in a film's crystallinity versus a change in the crystal orientation distribution. To definitively determine a change in crystallinity compared to the reorientation of crystals, the full reciprocal space must be mapped. The in-plane orientation distribution can be determined through an X-ray scan with azimuthal angle rotation (i.e.,  $\phi$ -scan). The  $\phi$ -scan can be used with a point detector or image detector. In the case of a point detector, a specific scattering peak is tracked with  $\phi$ -rotation. An image detector allows for a view of multiple scattering peaks as the film is rotated.<sup>30,147</sup> Importantly, the orientation distribution observed may depend on the scattering peak selected, particularly in semi-paracrystalline films.<sup>102</sup> In this case, the paracrystalline order depends on the crystallographic axis considered. Further method development is necessary to unpack changes in orientation, paracrystallinity, and degree of paracrystalline order (i.e., g-parameter)<sup>100</sup> in oriented films. Nevertheless, the orientation distribution of a scattering peak (e.g., (100)) from a phi-scan can then be used to determine a 2D order parameter similar to the UV-vis spectroscopy, given as  $S_{2D,crystal} = 2\langle \cos^2(\phi) \rangle - 1$ . Importantly, X-ray scattering provides the specific orientation distribution of the ordered polymer that meets the Bragg condition (i.e., crystalline material), while UV-vis provides an average orientation of all polymers in the film (crystalline and amorphous). Thus, by contrasting the 2D order parameters using these two methods, the alignment of the disordered fraction of the polymer can be captured.<sup>1,123</sup>

2D GIWAXS images of a strained P3HT film oriented parallel and perpendicular to the incident beam are given in Figure 10A.<sup>1</sup> Stronger in-plane scattering was seen for the lamellar (h00) series in the parallel direction compared to the perpendicular direction. In Figure 10B, high-resolution X-ray scattering using a point detector is presented, adjusted for each scattering vector position to maintain the scattering vector perpendicular or parallel to the direction of strain. These line scans at varying strains clearly show the increase in scattering for the perpendicular scattering vector as the degree of strain increases. A  $\phi$ -scan of the (200) scattering peak using a point detector is given in Figure 10C. Using the  $\phi$ -scan,  $S_{2D, crystal}$  was determined to be 0.84, representing a high level of crystal orientation with the backbone aligned in the direction of strain. In an oriented film, considering the scattering peaks that appear in the various orientations can assist in identifying the crystal structure.<sup>30</sup> For example, the crystal structure of poly[2,5-bis(3-tetradecylthiophen-2-yl)thieno[3,2-*b*]thiophene] (PBTTT) was determined by comparing scattering of biaxially oriented films with molecular mechanics modeling.<sup>150</sup> Similarly, Figure 10D displays parallel and perpendicular GIWAXS for a strain-aligned PBnDT-FTAZ film after heating.<sup>30</sup> Clear anisotropy can be seen between the parallel and perpendicular oriented film. The strain alignment also highlights an off-axis lamellar scattering series that assisted in defining a monoclinic unit cell.<sup>30</sup>

Although most X-ray scattering experiments are conducted on a substrate in grazing incidence, recently X-rays have been used on a strained film in a transmission geometry to help elucidate the origin of strain alignment.<sup>123</sup> The geometry of the experiment for hard X-rays is displayed in Figure 10E. Transmission X-ray scattering under strain can be used to investigate the alignment of crystalline domains (hard X-rays) or inform the orientation of the polymer backbone in crystallites (tender X-rays) during the straining process. For instance, in Figure 10F, as the degree of strain increased, the (h00) scattering increased perpendicular to the strain direction, while the (001) scattering increased along the straining direction.<sup>123</sup>

Near edge X-ray absorption fine structure (NEXAFS) utilizes the absorption of soft X-rays by core shell electrons to analyze the structure of a polymer film. NEXAFS can reveal the orientation of conjugated polymers through analysis of the C–C 1s  $\rightarrow \pi^*$  resonance. Here the 1s-  $\pi^*$  dipole moment is perpendicular to the conjugated ring in contrast to UV-vis  $\pi$ -  $\pi^*$  dipole moment that is the basis of UV-vis absorbance. Altering the X-ray angle of incidence as well as the in-plane azimuthal angle gives insight into the dichroism in the film. Utilizing surface-sensitive NEXAFS allows for the study of top-surface orientation and features, which can differ from bulk material. Comparing the anisotropy observed at the surface to bulk anisotropy is particularly useful when considering thickness dependence on alignment, as well as substrate effects on polymer templating. NEXAFS can be used to evaluate the in-plane orientation of the  $\pi$ -planes and the side chains and can add to valuable orientation information.<sup>141</sup> Similar to UV-vis spectroscopy, NEXAFS measures the average molecular orientation of all polymer populations.

### Microscopy

AFM is valuable for investigating surface characteristics of aligned films at the nanometer scale. In oriented polymer films, the surface may or may not exhibit clear signs of film alignment. However, there are several instances where AFM has been successfully employed to examine aligned conjugated polymers, revealing surface nanoribbons,<sup>151–153</sup> fibrils,<sup>147,154–157</sup> or terrace structures.<sup>30,151,153,158</sup> For example, P3HT has been shown to exhibit a fibril-type network at the surface after straining (Figure 11A), and PBnDT-FTAZ has exhibited a terrace-like structure following straining and heating (Figure 11B).<sup>1,30</sup>

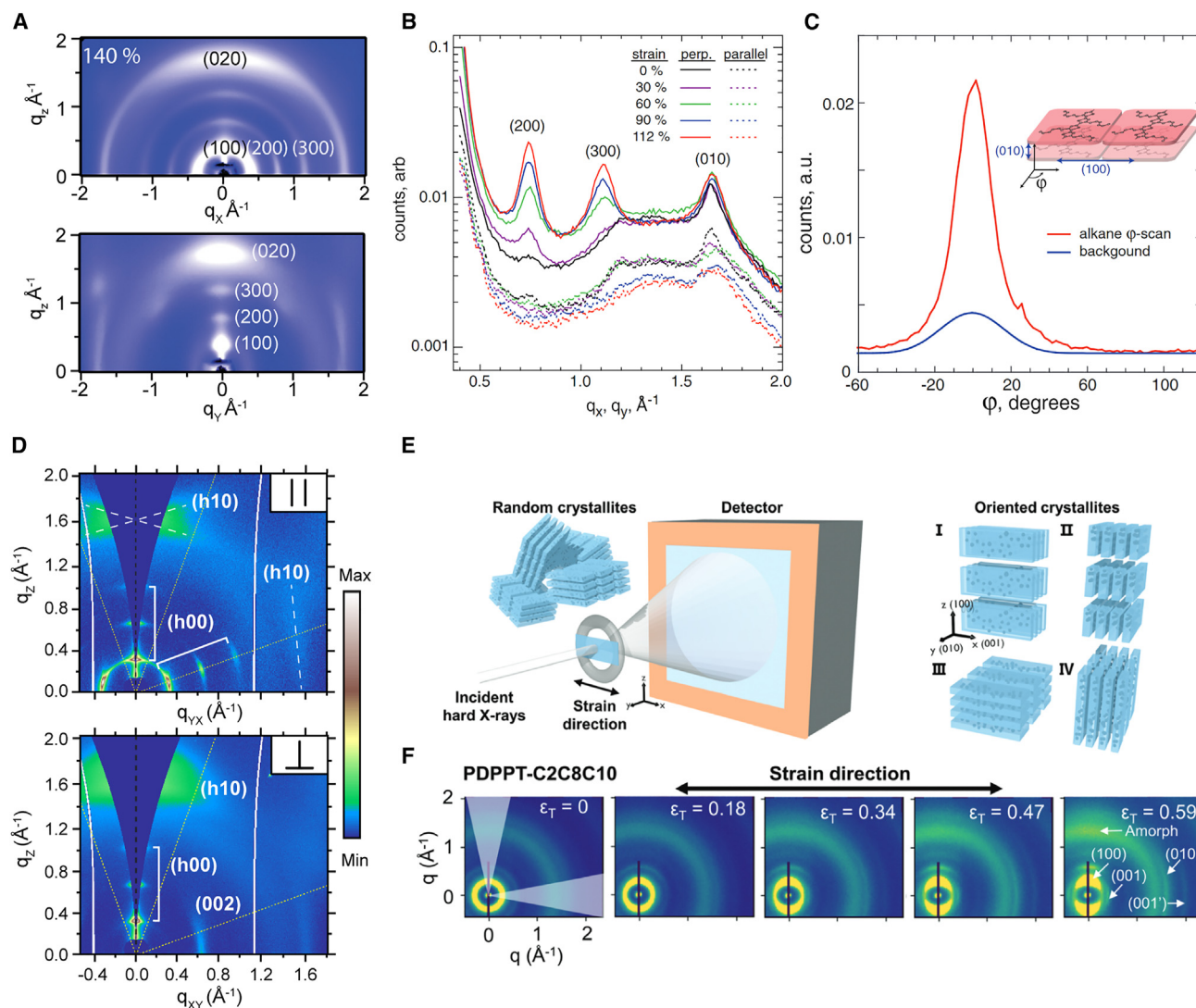


**Figure 10. X-ray scattering characterization of aligned polymer semiconductor films**

(A) GIWAXS images of P3HT films strained 140%, with the incident X-ray beam parallel (top) and perpendicular (bottom) to strain.<sup>1</sup>

(B) High-resolution line scans for P3HT films of various strain with the scattering vector oriented parallel and perpendicular to the strain direction.<sup>1</sup>

(C) X-ray diffraction  $\phi$ -scan of the in-plane (200) scattering peak for a P3HT film strained 112%. Reproduced with permission.<sup>1</sup> Copyright 2011, John Wiley and Sons.

(D) GIWAXS images of PbnDT-FTAZ films strained 40% and annealed at 270°C for 5 min, with the incident X-ray beam parallel (top) and perpendicular (bottom) to strain.<sup>30</sup>

(E and F) Schematic (E) and 2D scattering patterns (F) of wide-angle X-ray scattering on PDPPT-C2C8C10 films under varying strain. Reproduced with permission.<sup>123</sup> Copyright 2021, John Wiley and Sons.

TEM is a powerful tool to map the orientation distribution of oriented polymer films.

TEM can capture fine detail in a film (<nm), which can be useful in uncovering crystalline features and packing orientation and texture. High-resolution TEM (HRTEM), in particular, allows for direct visualization of chain alignment at the molecular level.<sup>159,160</sup>

While informative, TEM alone cannot fully elucidate the complete structure of a crystalline film since the transmission experimental geometry primarily provides information on in-plane features. It is often used in conjunction with diffraction techniques to obtain a more comprehensive structural understanding. One example has been shown by Biniek et al. with rub-aligned polythieno-[3,4-*b*]-thiophene-co-benzodithiophene

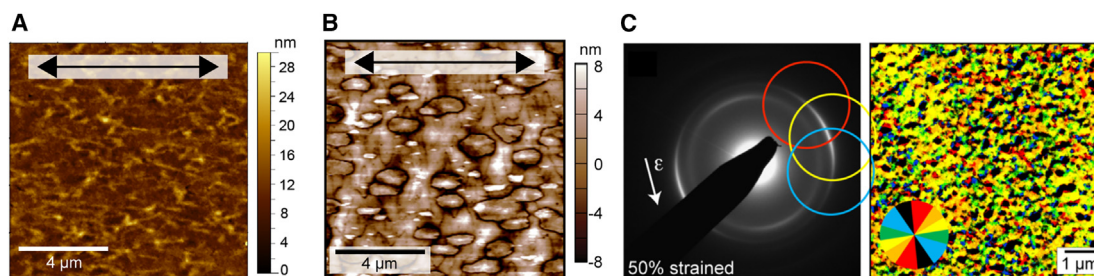


**Figure 11. Microscopy characterization of aligned polymer semiconductor films**

(A) AFM image of a P3HT film strained 140% and annealed at 180°C for 1 h featuring fibrillar surface morphology. Reproduced with permission.<sup>73</sup> Copyright 2014, John Wiley and Sons.

(B) AFM image of a PBnDT-FTAZ film strained 40% and annealed at 270°C for 1 min, featuring terraced surface morphology.<sup>30</sup>

(C) Electron diffraction patterns and dark-field TEM images for a PBTTT film strained 50%. The inset color map shows relative diffraction orientation associated with each color. Reproduced with permission.<sup>72</sup> Copyright 2015, American Chemical Society.

polymer film.<sup>161</sup> HRTEM was utilized alongside grazing incidence X-ray scattering to reveal primarily face-on domains. Indexed diffraction patterns matched the periodicity measured through HRTEM measurements, and an estimate for the crystallinity was proposed by measuring the relative area of the HRTEM image with face-on domains. Dark-field TEM (DF-TEM) is particularly effective in capturing grain boundaries and in-plane orientation in a polymer film.<sup>72,162</sup> This technique leverages electron diffraction characteristics, and image contrast is determined by in-plane diffraction orientation. By acquiring multiple images of the same film area with varying beam-tilt configurations, each pixel's intensity pattern can be correlated with the in-plane crystal orientation. Xue et al. demonstrated this approach when studying strained films of PBTTT using elevated temperatures.<sup>72</sup> As strain increased, grains in the terraced morphology of the film showed more uniform in-plane orientation versus unstrained films (Figure 11C). DF-TEM analysis can be valuable in characterizing the orientation of a film with a grain-boundary morphology, especially for films with higher degrees of crystallinity.

An extension of TEM that is particularly useful in the analysis of anisotropic conjugated polymer films is electron diffraction (ED). Similar to DF-TEM, ED captures diffracted electrons, but it employs a selected area aperture instead of an objective aperture. Consequently, ED provides a diffraction pattern rather than an image, revealing the crystallographic nature in a film. An illustration of an ED diffraction pattern is illustrated Figure 7. ED is helpful in unearthing the general orientation of crystallographic planes in the plane of the film but is unable to gather information about out-of-plane packing. Nonetheless, it is commonly used to characterize aligned films, allowing for isolation of very small areas of a film.

## Applications

### Enhanced charge carrier mobility

In-plane polymer alignment can result in anisotropic charge transport properties with enhanced charge mobility in the direction of backbone alignment.<sup>72</sup> This has led to interest in achieving high degrees of in-plane anisotropy in OFETs.<sup>25</sup> However, there is not a straightforward relationship between the degree of alignment achieved and the resulting mobility anisotropy, which can vary widely even with similar *DR*, as depicted in Figure 12A. This variability is due to confounding factors beyond ensemble average backbone alignment. In addition, alignment does not consistently show improved charge mobility compared to an isotropic film. This is because interchain charge transport bottlenecks can remain a limiting factor in charge mobility. Maintaining a sufficient level of chain connectivity is necessary for

enhancing charge transport, often through tie chains between aggregates or crystals.<sup>73</sup> Early efforts considering strain-aligned polymer semiconductors in OFETs were demonstrated by Dyreklev et al.<sup>14,15</sup> These demonstrations were based on stretching poly(3-octylthiophene) (POT) films on a polyethylene substrate and incorporating the strained films in OFETs. The stretching ratios in the POT films ranged from 1.3 to 4.5, and charge mobilities were measured in the direction both parallel and perpendicular to the applied strain. A clear linear trend was observed between the stretching ratio and mobility anisotropy. The mobility anisotropy increased from 1.46 at a stretching ratio of 1.3 to a maximum value of 4.5 at a stretching ratio of 4.5. Interestingly, there was no significant improvement in charge mobility between strained and unstrained OFETs. Yasuda et al. fabricated anisotropic OFETs using strained P3HT on a polypropylene (PP) substrate.<sup>163</sup> The P3HT/PP bilayer film was stretched at an elevated temperature of 170°C, and it reached a *DR* of 2.7 at the peak absorbance wavelength. A schematic of the OFET and polarized UV-vis absorbance spectra can be seen in Figure 12B. The field-effect hole mobility was reported to increase by 33% along the stretching direction compared to an unstrained film. Later work by Yasuda expanded the strain alignment technique to various materials, including P3HT, polydioctylfluorene (PFO), and poly[2-methoxy-5-(2'-ethylhexyloxy)-1,4-phenylene vinylene] (MEH-PPV).<sup>164</sup> In this work, the conjugated polymer films were spin coated on a PP substrate and strained at an elevated temperature to five times the initial length. Significant polymer alignment was observed, with a *DR* of 10.6 for P3HT, 4.1 for PFO, and 9.3 for MEH-PPV films. Seeing as P3HT is semi-crystalline, PFO is liquid-crystalline, and MEH-PPV is amorphous, it was argued that strain alignment was highly effective for orientation for most  $\pi$ -conjugated polymers. OFETs were fabricated with F<sub>4</sub>TCNQ<sup>-</sup> doped strained P3HT, achieving a field-effect hole mobility anisotropy of 3.4 and a conductivity anisotropy of 2.8.<sup>164</sup>

More recently, polymer semiconductor films were strained while on PDMS and then transfer printed to fabricate OFETs. Strained P3HT on PDMS by 168% followed by transfer printing on glass resulted in a *DR* of approximately 4.8 at peak absorption.<sup>1</sup> The mobility anisotropy in similarly fabricated OFETs reached a maximum of 9 with an applied strain of 140%, with greater mobility observed in the direction of strain. Figure 12C provides a summary of the change in orientation order parameter extracted from X-ray diffraction and UV-vis absorbance and the change mobility change with applied strain. It is observed that the change in mobility tracks closely with the change in backbone alignment of the crystalline material. A subsequent study in 2014 aimed to unearth the morphological origin of charge transport anisotropy in P3HT.<sup>73</sup> During this investigation, the impact of thermal annealing on the morphological and electrical characteristics of strained P3HT was examined. Interestingly, while marginal improvements were observed in optical anisotropy following annealing (*DR* increased from 4.4 to 5.4), charge mobility along the strain direction significantly decreased. This was attributed to the formation of sharp grains between oriented crystalline P3HT due to tie chain removal by thermal annealing. Furthermore, Wu et al. demonstrated a PDMS alignment strategy for evaluating the electrical characteristics of OFETs with stretched films.<sup>165</sup> In this approach, the semiconducting polymer film remained laminated to a PDMS slab for straining and characterization. This enabled testing varying levels of strain and multiple strain cycles with the same polymer film. They achieved a *DR* of approximately 1.6 and stable mobility for strains up to 100% for the most ductile polymer tested.<sup>165</sup> Strategies were developed to strain-align films, the typically brittle PBTTT and poly[4-(4,4-dihexadecyl-4Hcyclopenta[1,2-*b*:5,4-*b'*]dithiophen-2-yl)-alt[1,2,5]thiadiazolo [3,4-*c*]pyridine] (PCDTPT) films.<sup>72,166</sup> For PBTTT, heating the film to a temperature near its liquid-crystalline phase, the *COS* increases from ~3% at room temperature to

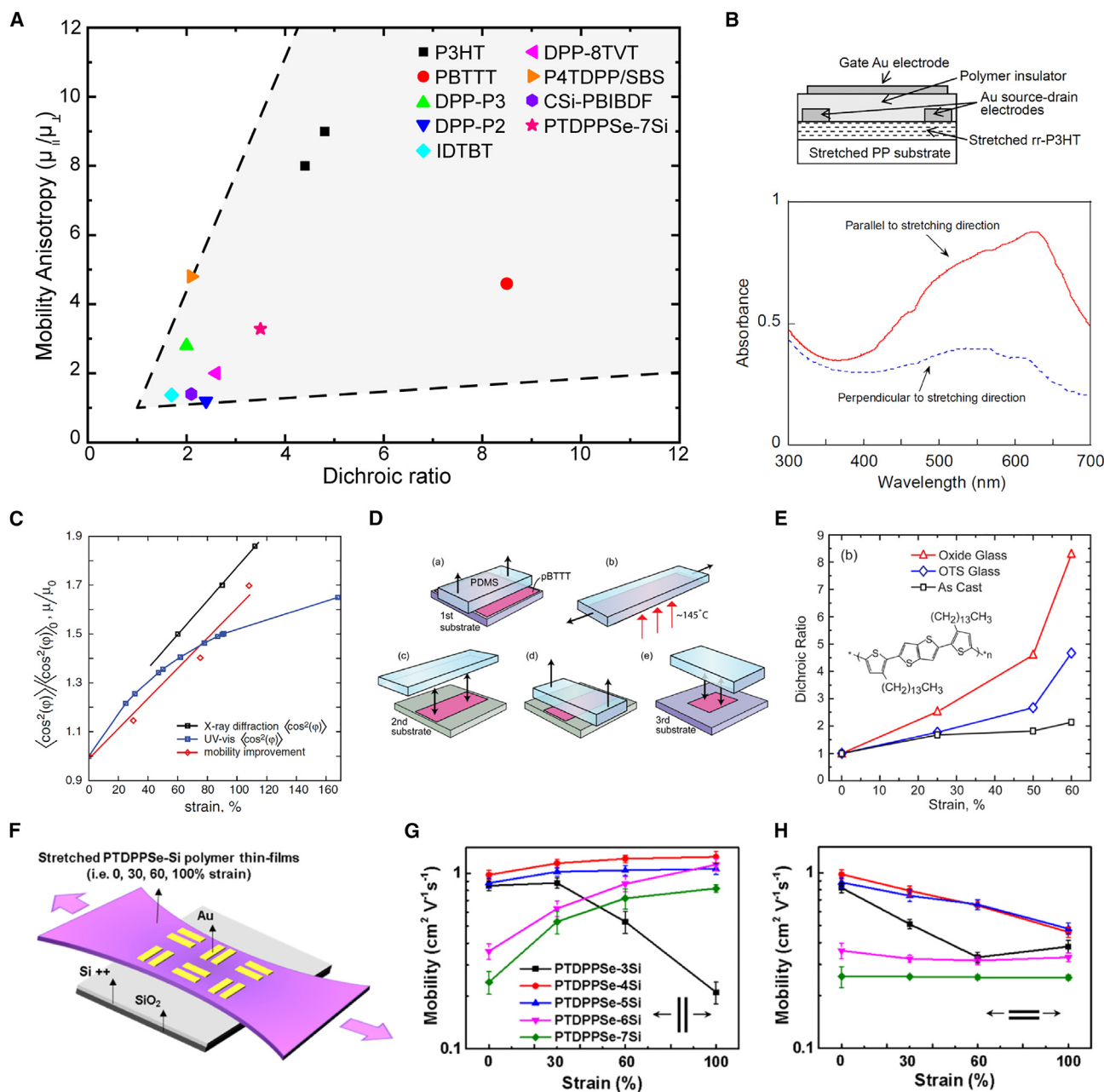


**Figure 12. Applications in enhancing charge carrier mobility**

(A) Mobility anisotropy vs. dichroic ratio for select polymer semiconductor films. A summary of the data is given in Table S3.

(B) Anisotropic OFET structure and polarized UV-vis absorbance spectra for strained rr-P3HT on a polypropylene substrate.<sup>163</sup>

(C) 2D order parameters (X-ray diffraction, UV-vis, and mobility) for P3HT at different strain levels. Reproduced with permission.<sup>1</sup> Copyright 2011, John Wiley and Sons.

(D and E) Alignment procedure (D) and DR versus strain (E) for pBTTT annealed on varying substrates. Reproduced with permission.<sup>72</sup> Copyright 2015, American Chemical Society.

(F–H) Device architecture of OFETs (F) using strained PTDPPSe-Si films, with charge mobilities (G) parallel and (H) perpendicular to the straining direction. Reproduced with permission.<sup>121</sup> Copyright 2022, American Chemical Society.

over 70%. A maximum DR of 8 was found for a film strained by 60% followed by a thermal annealing step, summarized in Figure 12D. Charge mobility along the strain direction reached a maximum of  $1.67 \text{ cm}^2 \text{ V}^{-1} \text{ s}^{-1}$ , which was among the highest

reported for this material. In the case of PCDTPT, which has a COS of less than 4%, film ductility was enhanced by blending the material with highly ductile P3HT. OFETs with the blend film preserved the charge transport character of PCDTPT, due to preferential segregation of the two materials while greatly increasing the ductility of the film. Straining the blend films results in a *DR* of approximately 3.75 and an increase in charge mobility from approximately  $1.0 \text{ cm}^2 \text{ V}^{-1} \text{ s}^{-1}$  to  $1.48 \text{ cm}^2 \text{ V}^{-1} \text{ s}^{-1}$ .

There have been numerous molecular design modifications to improve ductility as outlined above. Many of these demonstrated polymers have been strained and applied to OFETs.<sup>123,167</sup> One example has been grafting hybrid siloxane-based side chains onto a backbone of poly-diketo-pyrrolopyrrole-selenophene (PTDPPSe).<sup>121</sup> This significantly improved the stretchability of the polymer semiconductor, allowing for strains up to 100%. Charge mobility was shown to increase parallel to the straining direction, reaching values over  $1 \text{ cm}^2 \text{ V}^{-1} \text{ s}^{-1}$ . This improvement was attributed to the enhanced strain-induced alignment of the side-chain engineered polymers. Figures 12F–12H provides a schematic of the straining process along with the strain-dependent mobility anisotropy parallel and perpendicular to the straining direction.

#### Polarized emission

Oriented films with in-plane alignment exhibit a preference for emitting light with the electric field oriented parallel to the alignment direction. Grell et al. provided a thorough summary of initial experiments involving polarized luminescence with polymers.<sup>3</sup> Initially, many of these experiments utilized rubbing or textured substrates to induce alignment in polymer thin films. While rubbing and aligned substrates have proven effective for polymer alignment and polarized light emission, they often necessitate specific material requirements, such as a lyotropic or thermotropic liquid crystal polymer. Alternatively, some of the earliest applications of polarized emission used strain. The first report of polarized electroluminescence (EL) involved strain alignment of poly(3-(4-ocrylphenyl)-2,2'-bithiophene) (PTOPT) films on a polyethylene substrate.<sup>168</sup> The composite was strained to twice its initial length, and after integrating the film into an LED, the EL ratio was measured at 2.4. The associated spectral difference between the parallel and perpendicular emission is shown in Figure 13A. Anisotropic EL has also been shown on strain-oriented PPV.<sup>169,170</sup> Lemmer et al. demonstrated PPV films strained to 4 times their initial length, followed by the deposition of two gold electrodes.<sup>169</sup> EL was observed to be approximately 8 times stronger for polarization parallel to the stretch direction compared to perpendicular.

#### Polarization detection

Several instances of polarization-sensitive photodiodes have taken advantage of high-temperature rubbing<sup>55,172–176</sup> or a solution-phase approach<sup>177</sup> to align the polymer films. However, these methods can result in reduced detector performance, including lower responsivities and higher dark currents.<sup>55</sup> Alternatively, strain alignment has proven effective, given that the active layer films exhibit sufficient ductility to reach adequate strain levels for alignment. Strain alignment of bulk heterojunction (BHJ) films comprising a polymer donor and small molecule acceptor has been successfully demonstrated using blend films of P3HT:PCBM for polarization-sensitive photodetectors.<sup>2,19</sup> These films exhibited a maximum *DR* of approximately 6.5 at 100% strain, with a corresponding photocurrent anisotropy of 1.5.<sup>2</sup> Notably, the photodiode fill factor and open-circuit voltage remained unchanged under varying strain conditions, indicating that variation in short circuit current ( $J_{SC}$ ), driven by changes in absorption, was the primary factor in polarization response. The

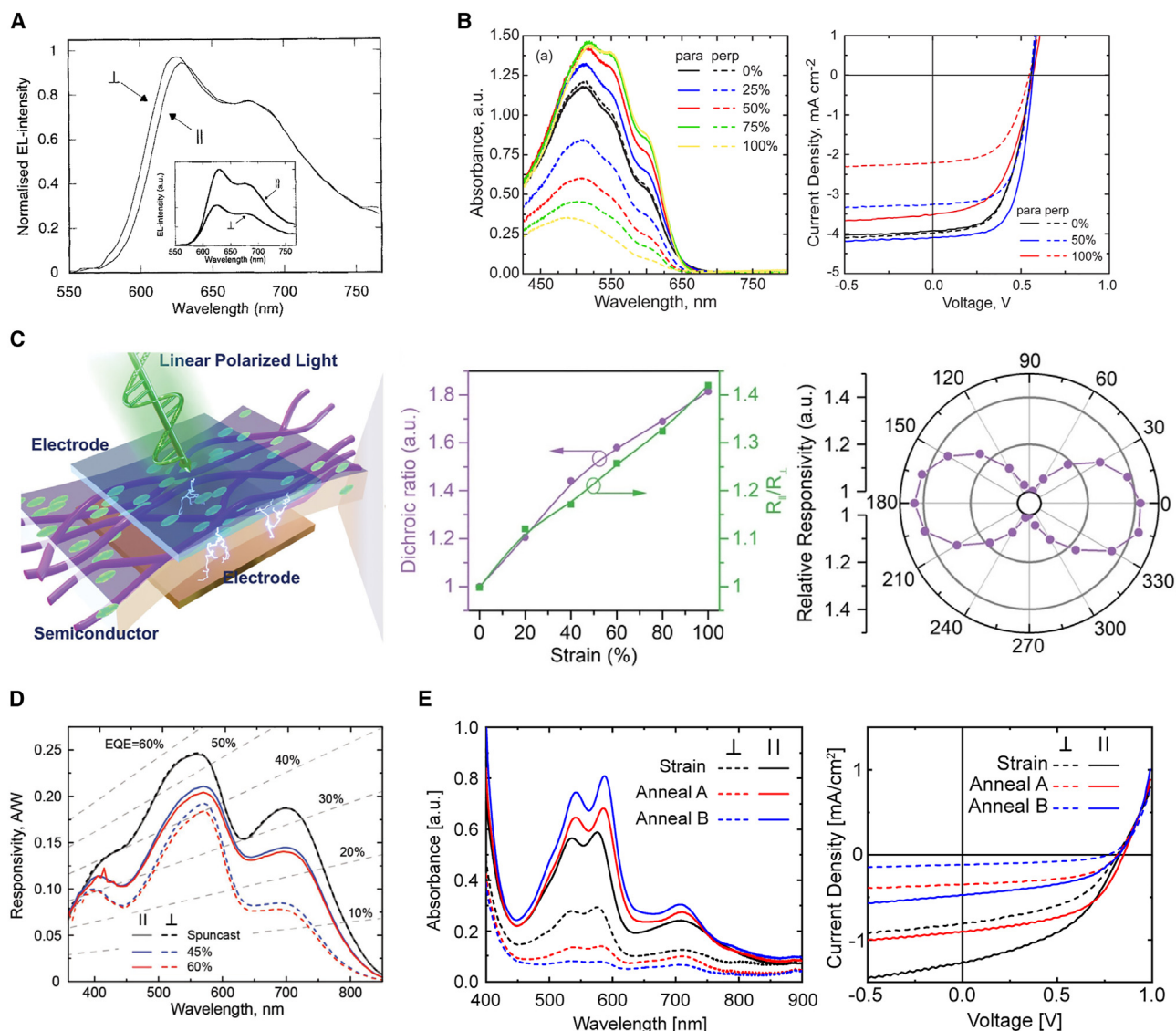


**Figure 13. Applications in polarized emission and detection**

(A) Polarized electroluminescence spectra of strain-aligned PTOPT LED. Reproduced with permission.<sup>168</sup> Copyright 2004, John Wiley and Sons.  
 (B) Polarized UV-vis spectra of strain-aligned P3HT:PCBM and current-voltage output of photodiode detectors utilizing the aligned film as the active layer. Reproduced with permission.<sup>2</sup> Copyright 2014, AIP Publishing.  
 (C) Schematic of polarization-resolved photodetector, strain-dependent dichroic ratio, and responsivity.<sup>171</sup>  
 (D) Spectral responsivity of photodiode detectors with strain-aligned PBnDT(FTAZ):P(NDI2OD-T2) films. Reproduced with permission.<sup>74</sup> Copyright 2018, John Wiley and Sons.  
 (E) Polarized UV-vis spectra of strained and annealed PBnDT(FTAZ):P(NDI2OD-T2) and current-voltage output of photodiode detectors utilizing the aligned film as the active layer. Reproduced with permission.<sup>55</sup> Copyright 2021, John Wiley and Sons.

polarized UV-vis spectra of strained P3HT:PCBM films and current-voltage characteristics of subsequent photodiode detectors are shown in Figure 13B. In this case, the small molecule PCBM does not show anisotropic optical properties, and the optical anisotropy is solely due to alignment of P3HT. It's worth noting that having a high fraction of small molecule acceptor in a blend film can often lead to brittle film behavior, which limits the potential for strain alignment.<sup>117,178</sup> However, recent approaches have shown that ductile polymer:small molecule BHJ films can be achieved through careful polymer design, precise control of film morphology, and

the addition of suitable additives.<sup>140,171,179</sup> A demonstration by Gao et al. utilized a BHJ of highly ductile PNTB6-Cl and the small molecule acceptor Y6.<sup>171</sup> The intrinsically stretchable blend film reached dichroic ratios of 1.82 at 100% strain, resulting in responsivity ratios reaching 1.42. The polarization-sensitive photodetectors maintained a high responsivity of  $0.45 \text{ A W}^{-1}$  and a specific detectivity over  $10^{12}$  Jones. Figure 13C provides an illustration of the detector, along with the blend film's *DR* and responsivity ratio versus strain and polarization-dependent relative responsivity.

The active layer can also consist of an all-polymer BHJ active layer. For instance, Sen et al. utilized a photoactive layer comprising PBnDT-FTAZ and P(NDI2OD-T2), capitalizing on sufficient ductility in the all-polymer blend, as well as complementary absorption spectra to enable polarization detection across the visible spectrum.<sup>74</sup> The resulting photodetectors displayed *DR* of approximately 2, along with photocurrent ratios of 1.4 under orthogonal polarized light after an application of 60% strain. Figure 13D depicts the responsivity of photodetectors with aligned PBnDT-FTAZ:P(NDI2OD-T2), showcasing both panchromatic and anisotropic responsivity. Along with polarization sensitivity, the photodetectors exhibited performance comparable to state-of-the-art all-polymer photodetectors with responsivity above  $0.2 \text{ A W}^{-1}$  and a 3-dB cutoff frequency of approximately 1 kHz. A recent demonstration has shown even greater absorption and photocurrent anisotropy utilizing aligned PBnDT-FTAZ:P(NDI2OD-T2).<sup>55</sup> Thermally annealing the strained films greatly enhanced chain alignment and polarization sensitivity, resulting in photocurrent ratios of nearly 4. Figure 13E shows the absorbance anisotropy under differing annealing conditions of the strained BHJ films, along with current-voltage characteristic of films integrated in a semitransparent photodiode configuration.

Polarization-sensitive OPDs have opened up new possibilities in polarimetry, or the quantification of the polarization state of light.<sup>19,20,171,175,180–182</sup> Quantifying polarized light has widespread applications ranging from atmospheric sensing to biomedical imaging.<sup>183,184</sup> Traditionally, the polarization state of light is mathematically represented by the Stokes parameters. Conventionally, determining the Stokes parameters is commonly achieved using a rotating polarizer in front of a detector or by using four spatially non-coincident detectors with stationary polarization filters in front of the individual cells. Hence, there is a trade-off between temporal and spatial resolution. Polarized OPDs can potentially overcome the challenges of these approaches by employing a stack of semitransparent polarized OPDs. The work by Gupta Roy et al. and Yang et al. demonstrated an accurate measurement of the Stokes parameters by stacking semitransparent, polarization-sensitive OPDs along a single optical path, allowing for a snapshot measurement of the Stokes parameters.<sup>19,20</sup>

## CONCLUSIONS

Strain is a simple and effective approach to orient polymer semiconductor films that can be used to understand fundamental characteristics of the film microstructure and electronic properties and be applied in devices to improve performance or introduce novel functionality. Strain has unique advantages over other alignment approaches including simplicity, alignment control, reproducibility, and effectiveness. As outlined in the numerous demonstrations in this report, the approach can be applied to a wide variety of polymer semiconductors, and transfer printing a strained film from an elastomer support can be realized with high fidelity on a variety of surfaces. Yet, polymer semiconductors must possess the requisite toughness and ductility to effectively strain the films while maintaining film cohesion and function.

In this report, we reviewed the molecular features (i.e., MW, backbone, side-chain characteristics, etc.) that contribute heavily to the mechanical behavior of conjugated polymer films. We also discuss the influence of film morphology and the neighboring substrate on the magnitude of strain that can be applied to the film prior to fracture.

It is important in any oriented organic semiconductor, strained or otherwise, that the film morphology is accurately characterized. In this review, we outline common practices for film characterization and highlight complexities that need to be considered in oriented film morphological analysis. This includes observed dichroism that may not be associated with polymer alignment, the additional X-ray diffraction information needed to determine the crystal orientation distribution and changes in crystallinity, and the additional ellipsometry measurements needed to accurately determine the anisotropic dielectric function. Importantly, many of the insights gained from strain alignment and characterization are integral to stretchable organic electronics where the film morphology will undergo similar changes under cyclic strain.

The use of strain alignment has been primarily applied in OFETs, OLEDs, and OPDs. Strain can be used to improve charge mobility in the direction of strain. However, this is not found to be universally the case due to intermolecular charge transport bottlenecks in the oriented film. In OLEDs, strain has resulted in polarized electroluminescence, and in OPDs, strain has resulted in polarization-dependent responsivity. In both OLEDs and OPDs, the polarization characteristics can be exploited for a range of applications including simplified display electronics to advanced spectro-polarimetric detection schemes. The demonstrations highlight the advantages of strain in device fabrication. The ability to strain a film on an elastomer support followed by transfer printing has been highly effective and allows for an additive manufacturing process that doesn't harm the polymer film or underlying device layers. While straining conjugated polymers has largely been conducted at a laboratory scale, this approach should be easily scaled. Stretching commodity polymers has been a standard practice in industry for decades, suggesting that similar large-scale approaches can be adopted for polymer semiconductors. As the appeal for conjugated polymers for electronic applications continues to grow, a successful integration of processing conditions, advanced conjugated polymer synthesis, and stable upscaling of current strain alignment processes can pave the way for innovative anisotropic and stretchable organic electronic devices.

### SUPPLEMENTAL INFORMATION

Supplemental information can be found online at <https://doi.org/10.1016/j.xcrp.2024.102076>.

### ACKNOWLEDGMENTS

This work is made possible by support from the National Science Foundation under grant no. 1809753 and the Office of Naval Research grant N00014-24-1-2101.

### AUTHOR CONTRIBUTIONS

Conceptualization, B.T.O., H.M.S., P.S., and N.B.; formal analysis, H.S.; writing – original draft, H.S.; writing – revisions, H.M.S., P.S., N.B., and B.T.O.; funding acquisition, B.T.O.; supervision, B.T.O.

## DECLARATION OF INTERESTS

P.S. is a current employee at First Solar, Inc. N.B. is a current employee at Intel Corporation.

## REFERENCES

- O'Connor, B., Kline, R.J., Conrad, B.R., Richter, L.J., Gundlach, D., Toney, M.F., and DeLongchamp, D.M. (2011). Anisotropic structure and charge transport in highly strain-aligned regioregular poly(3-hexylthiophene). *Adv. Funct. Mater.* 21, 3697–3705. <https://doi.org/10.1002/adfm.201100904>.
- Awartani, O., Kudenov, M.W., and O'Connor, B.T. (2014). Organic photovoltaic cells with controlled polarization sensitivity. *Appl. Phys. Lett.* 104, 1–5. <https://doi.org/10.1063/1.4868041>.
- Grell, M., and Bradley, D.D.C. (1999). Polarized luminescence from oriented molecular materials. *Adv. Mater.* 11, 895–905. [https://doi.org/10.1002/\(SICI\)1521-4095\(199908\)11:11<895::AID-ADMA895>3.0.CO;2-Y](https://doi.org/10.1002/(SICI)1521-4095(199908)11:11<895::AID-ADMA895>3.0.CO;2-Y).
- McElheny, V.K. (1999). *Biographical Memoirs, 77* (The National Academy Press), pp. 199–219. <https://doi.org/10.17226/9681>.
- Land, E.H., and Friedman, J.S. (1933). *Polarizing Refracting Bodies*.
- Land, E.H. (1941). *Light Polarizer and Process of Manufacturing the Same*.
- Land, E.H. (1951). Some Aspects of the Development of Sheet Polarizers. *JOSA* 41, 957–963. <https://doi.org/10.1364/JOSA.41.000957>.
- Land, E.H., and Rogers, H.G. (1939). *Light Polarizer*.
- Land, E.H., and Rogers, H.G. (1942). *Method of Manufacturing Light Polarizing Material*.
- Bennett, S., Cael, J.J., Kadaba, N.S., and Trapani, G.B. (1997). High-efficiency K-Sheet Polarizer.
- Osagawara, M., Funahashi, K., Demura, T., Hagiwara, T., and Iwata, K. (1986). Enhancement of electrical conductivity of polypyrrole by stretching. *Synth. Met.* 14, 61–69. [https://doi.org/10.1016/0379-6779\(86\)90127-X](https://doi.org/10.1016/0379-6779(86)90127-X).
- Nogami, Y., Pouget, J.P., and Ishiguro, T. (1994). Structure of highly conducting PF<sub>6</sub>-doped polypyrrole. *Synth. Met.* 62, 257–263. [https://doi.org/10.1016/0379-6779\(94\)90214-3](https://doi.org/10.1016/0379-6779(94)90214-3).
- Gustafsson, G., Inganäs, O., and Stafström, S. (1990). Optical anisotropy of neutral and doped poly(3-octylthiophene). *Solid State Commun.* 76, 203–208. [https://doi.org/10.1016/0038-1098\(90\)90543-K](https://doi.org/10.1016/0038-1098(90)90543-K).
- Dyreklev, P., Gustafsson, G., Inganäs, O., and Stubb, H. (1992). Aligned polymer chain field effect transistors. *Solid State Commun.* 82, 317–320. [https://doi.org/10.1016/0038-1098\(92\)90359-H](https://doi.org/10.1016/0038-1098(92)90359-H).
- Dyreklev, P., Gustafsson, G., Inganäs, O., and Stubb, H. (1993). Polymeric field effect transistors using oriented polymers. *Synth. Met.* 57, 4093–4098. [https://doi.org/10.1016/0379-6779\(93\)90563-C](https://doi.org/10.1016/0379-6779(93)90563-C).
- Goffri, S., Müller, C., Stingelin-Stutzmann, N., Breiby, D.W., Radano, C.P., Andreasen, J.W., Thompson, R., Janssen, R.A.J., Nielsen, M.M., Smith, P., and Sirringhaus, H. (2006). Multicomponent semiconducting polymer systems with low crystallization-induced percolation threshold. *Nat. Mater.* 5, 950–956. <https://doi.org/10.1038/nmat1779>.
- Müller, C., Goffri, S., Breiby, D.W., Andreasen, J.W., Chanzy, H.D., Janssen, R.A.J., Nielsen, M.M., Radano, C.P., Sirringhaus, H., Smith, P., and Stingelin-Stutzmann, N. (2007). Tough, semiconducting polyethylene-poly(3-hexylthiophene) diblock copolymers. *Adv. Funct. Mater.* 17, 2674–2679. <https://doi.org/10.1002/adfm.200601248>.
- Chabincyn, M.L., Salleo, A., Wu, Y., Liu, P., Ong, B.S., Heeney, M., and McCulloch, I. (2004). Lamination method for the study of interfaces in polymeric thin film transistors. *J. Am. Chem. Soc.* 126, 13928–13929. <https://doi.org/10.1021/ja044884a>.
- Roy, S.G., Awartani, O.M., Sen, P., O'Connor, B.T., and Kudenov, M.W. (2016). Intrinsic coincident linear polarimetry using stacked organic photovoltaics. *Opt Express* 24, 14737–14747. <https://doi.org/10.1364/oe.24.014737>.
- Yang, R., Sen, P., O'Connor, B.T., and Kudenov, M.W. (2017). Intrinsic coincident full-Stokes polarimeter using stacked organic photovoltaics. *Appl. Opt.* 56, 1768–1774. <https://doi.org/10.1364/ao.56.001768>.
- The Society of the Plastics Industry (1991). *In Plastics Engineering Handbook Of The Society Of The Plastics Industry, 5th ed.*, M.L. Berins, ed. (Springer Science & Business Media).
- Xu, X., Zhao, Y., and Liu, Y. (2023). Wearable Electronics Based on Stretchable Organic Semiconductors. *Small* 19, 2206309. <https://doi.org/10.1002/smll.202206309>.
- Lipomi, D.J., and Bao, Z. (2017). Stretchable and ultraflexible organic electronics. *MRS Bull.* 42, 93–97. <https://doi.org/10.1557/MRS.2016.325>.
- Savagatrup, S., Printz, A.D., O'Connor, T.F., Zaretski, A.V., and Lipomi, D.J. (2014). Molecularly stretchable electronics. *Chem. Mater.* 26, 3028–3041. <https://doi.org/10.1021/cm501021v>.
- Khim, D., Luzio, A., Bonacchini, G.E., Pace, G., Lee, M.J., Noh, Y.Y., and Caironi, M. (2018). Uniaxial Alignment of Conjugated Polymer Films for High-Performance Organic Field-Effect Transistors. *Adv. Mater.* 30, 1705463. <https://doi.org/10.1002/adma.201705463>.
- Pandey, M., Kumari, N., Nagamatsu, S., and Pandey, S.S. (2019). Recent advances in the orientation of conjugated polymers for organic field-effect transistors. *J. Mater. Chem. C Mater.* 7, 13323–13351. <https://doi.org/10.1039/c9tc04397g>.
- Memon, W.A., Zhang, Y., Zhang, J., Yan, Y., Wang, Y., and Wei, Z. (2022). Alignment of Organic Conjugated Molecules for High-Performance Device Applications. *Macromol. Rapid Commun.* 43, e2100931. <https://doi.org/10.1002/marc.202100931>.
- Deng, L., and Chen, G. (2021). Recent progress in tuning polymer oriented microstructures for enhanced thermoelectric performance. *Nano Energy* 80, 105448. <https://doi.org/10.1016/j.nanoen.2020.105448>.
- Brinkmann, M., Hartmann, L., Biniek, L., Tremel, K., and Kayunkid, N. (2014). Orienting semi-conducting  $\pi$ -conjugated polymers. *Macromol. Rapid Commun.* 35, 9–26. <https://doi.org/10.1002/marc.201300712>.
- Schrickx, H.M., Kashani, S., Buck, L., Ding, K., Rech, J.J., Flagg, L.Q., Li, R., Kudenov, M.W., You, W., Richter, L.J., et al. (2024). Exceptional Alignment in a Donor-Acceptor Conjugated Polymer via a Previously Unobserved Liquid Crystal Mesophase. *Adv. Funct. Mater.* 2315183. <https://doi.org/10.1002/adfm.202315183>.
- Hamidi-Sakr, A., Biniek, L., Bantignies, J.L., Maurin, D., Herrmann, L., Leclerc, N., Lévêque, P., Vijayakumar, V., Zimmermann, N., and Brinkmann, M. (2017). A Versatile Method to Fabricate Highly In-Plane Aligned Conducting Polymer Films with Anisotropic Charge Transport and Thermoelectric Properties: The Key Role of Alkyl Side Chain Layers on the Doping Mechanism. *Adv. Funct. Mater.* 27, 1–13. <https://doi.org/10.1002/adfm.201700173>.
- Polaroid Corporation Records (1936). *George W. Wheelwright III Demonstrating Polaroid Polarizing Lenses*.
- Le Berre, M., Chen, Y., and Baigl, D. (2009). From convective assembly to landau - Levich deposition of multilayered phospholipid films of controlled thickness. *Langmuir* 25, 2554–2557. <https://doi.org/10.1021/la803646e>.
- Lee, J., Han, A.R., Kim, J., Kim, Y., Oh, J.H., and Yang, C. (2012). Solution-processable ambipolar diketopyrrolopyrrole-selenophene polymer with unprecedentedly high hole and electron mobilities. *J. Am. Chem. Soc.* 134, 20713–20721. <https://doi.org/10.1021/ja308927g>.
- Lee, J., Han, A.R., Yu, H., Shin, T.J., Yang, C., and Oh, J.H. (2013). Boosting the ambipolar performance of solution-processable polymer semiconductors via hybrid side-chain engineering. *J. Am. Chem. Soc.* 135, 9540–9547. <https://doi.org/10.1021/ja403949g>.

36. Yabuuchi, Y., Minowa, Y., Kajii, H., Nagano, S., Fujii, A., and Ozaki, M. (2021). Direction-Selectable Ultra-Highly Oriented State of Donor-Acceptor Conjugated Polymer Induced by Slow Bar Coating Process. *Adv. Electron. Mater.* 7, 2100313. <https://doi.org/10.1002/aem.202100313>.
37. Schott, S., Gann, E., Thomsen, L., Jung, S.H., Lee, J.K., McNeill, C.R., and Siringhaus, H. (2015). Charge-Transport Anisotropy in a Uniaxially Aligned Diketopyrrolopyrrole-Based Copolymer. *Adv. Mater.* 27, 7356–7364. <https://doi.org/10.1002/adma.201502437>.
38. Shin, J., Hong, T.R., Lee, T.W., Kim, A., Kim, Y.H., Cho, M.J., Choi, D.H., Shin, J., Hong, T.R., Lee, T.W., et al. (2014). Template-Guided Solution-Shearing Method for Enhanced Charge Carrier Mobility in Diketopyrrolopyrrole-Based Polymer Field-Effect Transistors. *Adv. Mater.* 26, 6031–6035. <https://doi.org/10.1002/adma.201401179>.
39. Yuan, Y., Giri, G., Ayzner, A.L., Zoombelt, A.P., Mannsfeld, S.C.B., Chen, J., Nordlund, D., Toney, M.F., Huang, J., and Bao, Z. (2014). Ultra-high mobility transparent organic thin film transistors grown by an off-centre spin-coating method. *Nat. Commun.* 5, 3005–3009. <https://doi.org/10.1038/ncomms4005>.
40. Kim, N.K., Jang, S.Y., Pace, G., Caironi, M., Park, W.T., Khim, D., Kim, J., Kim, D.Y., and Noh, Y.Y. (2015). High-Performance Organic Field-Effect Transistors with Directionally Aligned Conjugated Polymer Film Deposited from Pre-Aggregated Solution. *Chem. Mater.* 27, 8345–8353. <https://doi.org/10.1021/acs.chemmater.5b03775>.
41. Lieser, G., Oda, M., Miteva, T., Meisel, A., Nothofer, H.G., Scherf, U., and Neher, D. (2000). Ordering, graphoepitaxial orientation, and conformation of a polyfluorene derivative of the “Hairy-Rod” type on an oriented substrate of polyimide. *Macromolecules* 33, 4490–4495. <https://doi.org/10.1021/ma9921652>.
42. Culligan, S.W., Geng, Y., Chen, S.H., Klubek, K., Vaeth, K.M., and Tang, C.W. (2003). Strongly polarized and efficient blue organic light-emitting diodes using monodisperse glassy nematic oligo(fluorene)s. *Adv. Mater.* 15, 1176–1180. <https://doi.org/10.1002/adma.200304972>.
43. Zhou, H., Jiang, S., and Yan, S. (2011). Epitaxial crystallization of poly(3-hexylthiophene) on a highly oriented polyethylene thin film from solution. *J. Phys. Chem. B* 115, 13449–13454. <https://doi.org/10.1021/jp205755r>.
44. Wittmann, J.C., and Smith, P. (1991). Highly oriented thin films of poly(tetrafluoroethylene) as a substrate for oriented growth of materials. *Nature* 352, 414–417. <https://doi.org/10.1038/352414a0>.
45. Brinkmann, M., and Wittmann, J. (2006). Orientation of regioregular poly(3-hexylthiophene) by directional solidification: A simple method to reveal the semicrystalline structure of a conjugated polymer. *Adv. Mater.* 18, 860–863. <https://doi.org/10.1002/adma.200501838>.
46. Brinkmann, M., and Rannou, P. (2007). Effect of molecular weight on the structure and morphology of oriented thin films of regioregular poly(3-hexylthiophene) grown by directional epitaxial solidification. *Adv. Funct. Mater.* 17, 101–108. <https://doi.org/10.1002/adfm.200600673>.
47. Morita, T., Singh, V., Nagamatsu, S., Oku, S., Takashima, W., and Kaneto, K. (2009). Enhancement of transport characteristics in poly(3-hexylthiophene) films deposited with floating film transfer method. *Appl. Phys. Express* 2, 111502. <https://doi.org/10.1143/APEX.2.111502>.
48. Binek, L., Pouget, S., Djurado, D., Gonther, E., Tremel, K., Kayunkid, N., Zaborova, E., Crespo-Monteiro, N., Boyron, O., Leclerc, N., et al. (2014). High-temperature rubbing: A versatile method to align  $\pi$ -conjugated polymers without alignment substrate. *Macromolecules* 47, 3871–3879. <https://doi.org/10.1021/ma500762x>.
49. Van Aerle, N.A.J.M., Barmantlo, M., and Hollering, R.W.J. (1993). Effect of rubbing on the molecular orientation within polyimide orienting layers of liquid-crystal displays. *J. Appl. Phys.* 74, 3111–3120. <https://doi.org/10.1063/1.354577>.
50. van Aerle, N.A.J.M., and Tol, A.J.W. (1994). Molecular Orientation in Rubbed Polyimide Alignment Layers Used for Liquid-Crystal Displays. *Macromolecules* 27, 6520–6526. <https://doi.org/10.1021/ma00100a042>.
51. Sariciftci, N.S., Lemmer, U., Vacar, D., Heeger, A.J., and Janssen, R.A.J. (1996). Polarized photoluminescence of oligothiophenes in nematic liquid crystalline matrices. *Adv. Mater.* 8, 651–654. <https://doi.org/10.1002/adma.19960080810>.
52. Kim, D., Lee, S.B., Kim, M.J., Lee, J., Chung, S., Ok, E., Lee, G., Min, J., Cho, K., and Kang, B. (2023). Low-Temperature Alignment of Conjugated Polymers by Plasticizer-Aided Physical Rubbing. *Small Methods* 7, 2300256. <https://doi.org/10.1002/smt.202300256>.
53. Kajija, D., Ozawa, S., Koganezawa, T., and Saitow, K.I. (2015). Enhancement of out-of-plane mobility in P3HT film by rubbing: Aggregation and planarity enhanced with low regioregularity. *J. Phys. Chem. C* 119, 7987–7995. <https://doi.org/10.1021/jp510675r>.
54. Guchait, S., Zhong, Y., and Brinkmann, M. (2023). High-Temperature Rubbing: An Effective Method to Fabricate Large-Scale Aligned Semiconducting and Conducting Polymer Films for Applications in Organic Electronics. *Macromolecules* 56, 6733–6757. <https://doi.org/10.1021/acs.macromol.3c01073>.
55. Schrickx, H.M., Sen, P., Booth, R.E., Altaqui, A., Burlison, J., Rech, J.J., Lee, J.-W., Biliroglu, M., Gundogdu, K., Kim, B.J., et al. (2021). Ultra-High Alignment of Polymer Semiconductor Blends Enabling Photodetectors with Exceptional Polarization Sensitivity. *Adv. Funct. Mater.* 32, 2105820. <https://doi.org/10.1002/adfm.202105820>.
56. Misaki, M., Ueda, Y., Nagamatsu, S., Chikamatsu, M., Yoshida, Y., Tanigaki, N., and Yase, K. (2005). Highly polarized polymer light-emitting diodes utilizing friction-transferred poly(9,9-dioctylfluorene) thin films. *Appl. Phys. Lett.* 87, 1–3. <https://doi.org/10.1063/1.2142082>.
57. Nagamatsu, S., Misaki, M., Chikamatsu, M., Kimura, T., Yoshida, Y., Azumi, R., Tanigaki, N., and Yase, K. (2007). Crystal structure of friction-transferred poly(2,5-dioctyloxy-1,4-phenylenevinylene). *J. Phys. Chem. B* 111, 4349–4354. <https://doi.org/10.1021/jp067555m>.
58. Ichino, Y., Takada, N., Tanigaki, N., Kaito, A., Yoshida, M., Yokokawa, S., and Sakurai, H. (2000). Polarized electroluminescence from a uniaxially oriented polysilane thin film. *Thin Solid Films* 376, 220–224. [https://doi.org/10.1016/S0040-6090\(00\)01409-7](https://doi.org/10.1016/S0040-6090(00)01409-7).
59. Motamedi, F., Ihn, K.J., Fenwick, D., Wittmann, J.-C., and Smith, P. (1994). Polymer friction-transfer layers as orienting substrates. *J. Polym. Sci. B Polym. Phys.* 32, 453–457. <https://doi.org/10.1002/polb.1994.090320306>.
60. Tanigaki, N., Yase, K., and Kaito, A. (1996). Oriented films of insoluble polymers by the friction technique. *Thin Solid Films* 273, 263–266. [https://doi.org/10.1016/0040-6090\(95\)07001-X](https://doi.org/10.1016/0040-6090(95)07001-X).
61. Kumari, N., Pandey, M., Nagamatsu, S., Nakamura, M., and Pandey, S.S. (2020). Investigation and Control of Charge Transport Anisotropy in Highly Oriented Friction-Transferred Polythiophene Thin Films. *ACS Appl. Mater. Interfaces* 12, 11876–11883. <https://doi.org/10.1021/acsami.9b23345>.
62. Carlson, A., Bowen, A.M., Huang, Y., Nuzzo, R.G., and Rogers, J.A. (2012). Transfer printing techniques for materials assembly and micro/nanodevice fabrication. *Adv. Mater.* 24, 5284–5318. <https://doi.org/10.1002/adma.201201386>.
63. Li, D., and Guo, L.J. (2006). Micron-scale organic thin film transistors with conducting polymer electrodes patterned by polymer inking and stamping. *Appl. Phys. Lett.* 88, 063513. <https://doi.org/10.1063/1.2168669>.
64. Yim, K.H., Zheng, Z., Liang, Z., Friend, R.H., Huck, W.T.S., and Kim, J.S. (2008). Efficient conjugated-polymer optoelectronic devices fabricated by thin-film transfer-printing technique. *Adv. Funct. Mater.* 18, 1012–1019. <https://doi.org/10.1002/adfm.200701321>.
65. Li, D., and Guo, L.J. (2008). Organic thin film transistors and polymer light-emitting diodes patterned by polymer inking and stamping. *J. Phys. D Appl. Phys.* 41, 105115. <https://doi.org/10.1088/0022-3727/41/10/105115>.
66. Kim, H., Yoon, B., Sung, J., Choi, D.G., and Park, C. (2008). Micropatterning of thin P3HT films via plasma enhanced polymer transfer printing. *J. Mater. Chem.* 18, 3489–3495. <https://doi.org/10.1039/b807285j>.
67. Sen, P., Xiong, Y., Zhang, Q., Park, S., You, W., Ade, H., Kudenov, M.W., and O'Connor, B.T. (2018). Shear-Enhanced Transfer Printing of Conducting Polymer Thin Films. *ACS Appl. Mater. Interfaces* 10, 31560–31567. <https://doi.org/10.1021/acsami.8b09968>.

68. Zabow, G. (2022). Reflow transfer for conformal three-dimensional microprinting. *Science* (1979 378, 894–898).
69. Sun, T., Song, R., Balar, N., Sen, P., Kline, R.J., and O'Connor, B.T. (2019). Impact of Substrate Characteristics on Stretchable Polymer Semiconductor Behavior. *ACS Appl. Mater. Interfaces* 11, 3280–3289. <https://doi.org/10.1021/acsami.8b16457>.
70. Kim, C., Cao, Y., Soboyejo, W.O., and Forrest, S.R. (2005). Patterning of active organic materials by direct transfer for organic electronic devices. *J. Appl. Phys.* 97, 113512. <https://doi.org/10.1063/1.1900285>.
71. Song, R., Yao, S., Liu, Y., Wang, H., Dong, J., Zhu, Y., and O'Connor, B.T. (2020). Facile Approach to Fabricating Stretchable Organic Transistors with Laser-Patterned Ag Nanowire Electrodes. *ACS Appl. Mater. Interfaces* 12, 50675–50683. <https://doi.org/10.1021/acsami.0c15339>.
72. Xue, X., Chandler, G., Zhang, X., Kline, R.J., Fei, Z., Heeney, M., Diemer, P.J., Jurchescu, O.D., and O'Connor, B.T. (2015). Oriented Liquid Crystalline Polymer Semiconductor Films with Large Ordered Domains. *ACS Appl. Mater. Interfaces* 7, 26726–26734. <https://doi.org/10.1021/acsami.5b08710>.
73. O'Connor, B.T., Reid, O.G., Zhang, X., Kline, R.J., Richter, L.J., Gundlach, D.J., DeLongchamp, D.M., Toney, M.F., Kopidakis, N., and Rumbles, G. (2014). Morphological origin of charge transport anisotropy in aligned polythiophene thin films. *Adv. Funct. Mater.* 24, 3422–3431. <https://doi.org/10.1002/adfm.201303351>.
74. Sen, P., Yang, R., Rech, J.J., Feng, Y., Ho, C.H.Y., Huang, J., So, F., Kline, R.J., You, W., Kudenov, M.W., et al. (2019). Panchromatic All-Polymer Photodetector with Tunable Polarization Sensitivity. *Adv. Opt. Mater.* 7, 1–9. <https://doi.org/10.1002/adom.201801346>.
75. Tien, H.C., Huang, Y.W., Chiu, Y.C., Cheng, Y.H., Chueh, C.C., and Lee, W.Y. (2021). Intrinsically stretchable polymer semiconductors: molecular design, processing and device applications. *J. Mater. Chem. C Mater.* 9, 2660–2684. <https://doi.org/10.1039/d0tc06059c>.
76. Zheng, Y., Zhang, S., Tok, J.B.H., and Bao, Z. (2022). Molecular Design of Stretchable Polymer Semiconductors: Current Progress and Future Directions. *J. Am. Chem. Soc.* 144, 4699–4715. <https://doi.org/10.1021/jacs.2c00072>.
77. O'Connor, B.T., Awartani, O.M., and Balar, N. (2017). Morphological considerations of organic electronic films for flexible and stretchable devices. *MRS Bull.* 42, 108–114. <https://doi.org/10.1557/mrs.2017.6>.
78. Rodriguez, D., Kim, J.H., Root, S.E., Fei, Z., Boufflet, P., Heeney, M., Kim, T.S., and Lipomi, D.J. (2017). Comparison of Methods for Determining the Mechanical Properties of Semiconducting Polymer Films for Stretchable Electronics. *ACS Appl. Mater. Interfaces* 9, 8855–8862. <https://doi.org/10.1021/acsami.6b16115>.
79. Awartani, O., Lemanski, B.I., Ro, H.W., Richter, L.J., De Longchamp, D.M., and O'Connor, B.T. (2013). Correlating stiffness, ductility, and morphology of polymer:Fullerene films for solar cell applications. *Adv. Energy Mater.* 3, 399–406. <https://doi.org/10.1002/aenm.201200595>.
80. Alkhadra, M.A., Root, S.E., Hilby, K.M., Rodriquez, D., Sugiyama, F., and Lipomi, D.J. (2017). Quantifying the Fracture Behavior of Brittle and Ductile Thin Films of Semiconducting Polymers. *Chem. Mater.* 29, 10139–10149. <https://doi.org/10.1021/acs.chemmater.7b03922>.
81. Chung, J.Y., Nolte, A.J., and Stafford, C.M. (2011). Surface Wrinkling: A Versatile Platform for Measuring Thin-Film Properties. *Adv. Mater.* 23, 349–368. <https://doi.org/10.1002/ADMA.201001759>.
82. Stafford, C.M., Harrison, C., Beers, K.L., Karim, A., Amis, E.J., Vanlandingham, M.R., Kim, H.C., Volksen, W., Miller, R.D., and Simonyi, E.E. (2004). A buckling-based metrology for measuring the elastic moduli of polymeric thin films. *Nat. Mater.* 3, 545–550. <https://doi.org/10.1038/nmat1175>.
83. O'Connor, B., Chan, E.P., Chan, C., Conrad, B.R., Richter, L.J., Kline, R.J., Heeney, M., McCulloch, I., Soles, C.L., and DeLongchamp, D.M. (2010). Correlations between mechanical and electrical properties of polythiophenes. *ACS Nano* 4, 7538–7544. <https://doi.org/10.1021/nn1018768>.
84. Chung, J.Y., Douglas, J.F., and Stafford, C.M. (2017). A wrinkling-based method for investigating glassy polymer film relaxation as a function of film thickness and temperature. *J. Chem. Phys.* 147, 154902. <https://doi.org/10.1063/1.5006949>.
85. Song, R., Schrickx, H., Balar, N., Siddika, S., Sheikh, N., and O'Connor, B.T. (2020). Unveiling the Stress-Strain Behavior of Conjugated Polymer Thin Films for Stretchable Device Applications. *Macromolecules* 53, 1988–1997. <https://doi.org/10.1021/acs.macromol.9b02573>.
86. Kim, T., Kim, J.H., Kang, T.E., Lee, C., Kang, H., Shin, M., Wang, C., Ma, B., Jeong, U., Kim, T.S., and Kim, B.J. (2015). Flexible, highly efficient all-polymer solar cells. *Nat. Commun.* 6, 8547. <https://doi.org/10.1038/ncomms9547>.
87. Kim, J.H., Nizami, A., Hwangbo, Y., Jang, B., Lee, H.J., Woo, C.S., Hyun, S., and Kim, T.S. (2013). Tensile testing of ultra-thin films on water surface. *Nat. Commun.* 4, 2520–2526. <https://doi.org/10.1038/ncomms3520>.
88. Kim, H.J., Kim, J.H., Ryu, J.H., Kim, Y., Kang, H., Lee, W.B., Kim, T.S., and Kim, B.J. (2014). Architectural engineering of rod-coil compatibilizers for producing mechanically and thermally stable polymer solar cells. *ACS Nano* 8, 10461–10470. <https://doi.org/10.1021/nn503823z>.
89. Liu, Y., Chen, Y.C., Hutchens, S., Lawrence, J., Emrick, T., and Crosby, A.J. (2015). Directly Measuring the Complete Stress-Strain Response of Ultrathin Polymer Films. *Macromolecules* 48, 6534–6540. <https://doi.org/10.1021/acs.macromol.5b01473>.
90. Chen, A.X., Kleinschmidt, A.T., Choudhary, K., and Lipomi, D.J. (2020). Beyond Stretchability: Strength, Toughness, and Elastic Range in Semiconducting Polymers. *Chem. Mater.* 32, 7582–7601. <https://doi.org/10.1021/acs.chemmater.0c03019>.
91. Zhang, S., Galuska, L.A., and Gu, X. (2022). Water-assisted mechanical testing of polymeric thin-films. *J. Polym. Sci.* 60, 1108–1129. <https://doi.org/10.1002/pol.20210281>.
92. Bay, R.K., and Crosby, A.J. (2019). Uniaxial Extension of Ultrathin Freestanding Polymer Films. *ACS Macro Lett.* 8, 1080–1085. <https://doi.org/10.1021/acsmacrolett.9b00408>.
93. Park, H., Ma, B.S., Kim, Y., Lee, D., Li, S., Kim, H.J., Kim, T.-S., and Kim, B.J. (2023). Direct Measurement of the Thermomechanical Properties of Poly(3-hexylthiophene) Thin Films on Ionic Liquid Surfaces. *Macromolecules* 56, 1633–1642. <https://doi.org/10.1021/acs.macromol.2c02275>.
94. Galuska, L.A., Ocheje, M.U., Ahmad, Z.C., Rondeau-Gagné, S., and Gu, X. (2022). Elucidating the Role of Hydrogen Bonds for Improved Mechanical Properties in a High-Performance Semiconducting Polymer. *Chem. Mater.* 34, 2259–2267. <https://doi.org/10.1021/acs.chemmater.1c04055>.
95. Galuska, L.A., Muckley, E.S., Cao, Z., Ehlenberg, D.F., Qian, Z., Zhang, S., Rondeau-Gagné, S., Phan, M.D., Ankner, J.F., Ivanov, I.N., and Gu, X. (2021). SMART transfer method to directly compare the mechanical response of water-supported and free-standing ultrathin polymeric films. *Nat. Commun.* 12, 2347. <https://doi.org/10.1038/s41467-021-22473-w>.
96. Balar, N., Siddika, S., Kashani, S., Peng, Z., Rech, J.J., Ye, L., You, W., Ade, H., and O'Connor, B.T. (2020). Role of Secondary Thermal Relaxations in Conjugated Polymer Film Toughness. *Chem. Mater.* 32, 6540–6549. <https://doi.org/10.1021/acs.chemmater.0c01910>.
97. Bartczak, Z., and Galeski, A. (2010). Plasticity of semicrystalline polymers. *Macromol. Symp.* 294, 67–90. <https://doi.org/10.1002/masy.201050807>.
98. Sharma, A., Pan, X., Bjuggren, J.M., Gedefaw, D., Xu, X., Kroon, R., Wang, E., Campbell, J.A., Lewis, D.A., and Andersson, M.R. (2019). Probing the Relationship between Molecular Structures, Thermal Transitions, and Morphology in Polymer Semiconductors Using a Woven Glass-Mesh-Based DMTA Technique. *Chem. Mater.* 31, 6740–6749. <https://doi.org/10.1021/acs.chemmater.9b01213>.
99. Balar, N., Rech, J.J., Siddika, S., Song, R., Schrickx, H.M., Sheikh, N., Ye, L., Megret Bonilla, A., Awartani, O., Ade, H., et al. (2021). Resolving the Molecular Origin of Mechanical Relaxations in Donor-Acceptor Polymer Semiconductors. *Adv. Funct. Mater.* 32, 2105597. <https://doi.org/10.1002/adfm.202105597>.
100. Peng, Z., Ye, L., and Ade, H. (2022). Understanding, quantifying, and controlling the molecular ordering of semiconducting polymers: from novices to experts and amorphous to perfect crystals. *Mater. Horiz.* 9,

- 577–606. <https://doi.org/10.1039/D0MH00837K>.
101. Qian, Z., Galuska, L., McNutt, W.W., Ocheje, M.U., He, Y., Cao, Z., Zhang, S., Xu, J., Hong, K., Goodman, R.B., et al. (2019). Challenge and Solution of Characterizing Glass Transition Temperature for Conjugated Polymers by Differential Scanning Calorimetry. *J. Polym. Sci. B Polym. Phys.* 57, 1635–1644. <https://doi.org/10.1002/polb.24889>.
  102. Marina, S., Gutierrez-Fernandez, E., Gutierrez, J., Gobbi, M., Ramos, N., Solano, E., Rech, J., You, W., Hueso, L., Tercjak, A., et al. (2022). Semi-paracrystallinity in semi-conducting polymers. *Mater. Horiz.* 9, 1196–1206. <https://doi.org/10.1039/d1mh01349a>.
  103. Fleischmann, E.K., and Zentel, R. (2013). Liquid-Crystalline Ordering as a Concept in Materials Science: From Semiconductors to Stimuli-Responsive Devices. *Angew. Chem. Int. Ed. Engl.* 52, 8810–8827. <https://doi.org/10.1002/anie.201300371>.
  104. Gu, K., Onorato, J.W., Luscombe, C.K., and Loo, Y.L. (2020). The Role of Tie Chains on the Mechano-Electrical Properties of Semiconducting Polymer Films. *Adv. Electron. Mater.* 6, 1901070. <https://doi.org/10.1002/aeml.201901070>.
  105. Oleinik, E.F., Rudnev, S.N., and Salamatina, O.B. (2007). Evolution in concepts concerning the mechanism of plasticity in solid polymers after the 1950s. *Polym. Sci. Ser. A* 49, 1302–1327. <https://doi.org/10.1134/S0965545X07120073>.
  106. Roth, B., Savagatrup, S., V de los Santos, N., Hagemann, O., Carlé, J.E., Helgesen, M., Livi, F., Bundgaard, E., Søndergaard, R.R., Krebs, F.C., and Lipomi, D.J. (2016). Mechanical Properties of a Library of Low-Band-Gap Polymers. *Chem. Mater.* 28, 2363–2373. <https://doi.org/10.1021/acs.chemmater.6b00525>.
  107. Savagatrup, S., Printz, A.D., Rodríguez, D., and Lipomi, D.J. (2014). Best of both worlds: Conjugated polymers exhibiting good photovoltaic behavior and high tensile elasticity. *Macromolecules* 47, 1981–1992. <https://doi.org/10.1021/ma500286d>.
  108. Ashizawa, M., Zheng, Y., Tran, H., and Bao, Z. (2020). Intrinsically stretchable conjugated polymer semiconductors in field effect transistors. *Prog. Polym. Sci.* 100, 101181. <https://doi.org/10.1016/j.progpolymsci.2019.101181>.
  109. Root, S.E., Savagatrup, S., Printz, A.D., Rodríguez, D., and Lipomi, D.J. (2017). Mechanical Properties of Organic Semiconductors for Stretchable, Highly Flexible, and Mechanically Robust Electronics. *Chem. Rev.* 117, 6467–6499. <https://doi.org/10.1021/acs.chemrev.7b00003>.
  110. Capaccio, G., and Ward, I.M. (1974). Preparation of ultra-high modulus linear polyethylenes; effect of molecular weight and molecular weight distribution on drawing behaviour and mechanical properties. *Polymer (Guildf)* 15, 233–238. [https://doi.org/10.1016/0032-3861\(74\)90038-X](https://doi.org/10.1016/0032-3861(74)90038-X).
  111. Nunes, R.W., Martin, J.R., and Johnson, J.F. (1982). Influence of molecular weight and molecular weight distribution on mechanical properties of polymers. *Polym. Eng. Sci.* 22, 205–228. <https://doi.org/10.1002/PEN.760220402>.
  112. Koch, F.P.V., Rivnay, J., Foster, S., Müller, C., Downing, J.M., Buchaca-Domingo, E., Westacott, P., Yu, L., Yuan, M., Baklar, M., et al. (2013). The impact of molecular weight on microstructure and charge transport in semicrystalline polymer semiconductors—poly(3-hexylthiophene), a model study. *Prog. Polym. Sci.* 38, 1978–1989. <https://doi.org/10.1016/J.PROGPOLYMSCI.2013.07.009>.
  113. Balar, N., and O'Connor, B.T. (2017). Correlating Crack Onset Strain and Cohesive Fracture Energy in Polymer Semiconductor Films. *Macromolecules* 50, 8611–8618. <https://doi.org/10.1021/acs.macromol.7b01282>.
  114. Bruner, C., and Dauskardt, R. (2014). Role of molecular weight on the mechanical device properties of organic polymer solar cells. *Macromolecules* 47, 1117–1121. <https://doi.org/10.1021/ma402215j>.
  115. Tummla, N.R., Risko, C., Bruner, C., Dauskardt, R.H., and Brédas, J.-L. (2015). Entanglements in P3HT and their influence on thin-film mechanical properties: Insights from molecular dynamics simulations. *J. Polym. Sci. B Polym. Phys.* 53, 934–942. <https://doi.org/10.1002/POLB.23722>.
  116. Balar, N., Rech, J.J., Henry, R., Ye, L., Ade, H., You, W., and O'Connor, B.T. (2019). The Importance of Entanglements in Optimizing the Mechanical and Electrical Performance of All-Polymer Solar Cells. *Chem. Mater.* 31, 5124–5132. <https://doi.org/10.1021/acs.chemmater.9b01011>.
  117. Choi, J., Kim, W., Kim, S., Kim, T.-S., and Kim, B.J. (2019). Influence of Acceptor Type and Polymer Molecular Weight on the Mechanical Properties of Polymer Solar Cells. *Chem. Mater.* 31, 9057–9069. <https://doi.org/10.1021/acs.chemmater.9b03333>.
  118. Choi, J., Kim, W., Kim, D., Kim, S., Chae, J., Choi, S.Q., Kim, F.S., Kim, T.S., and Kim, B.J. (2019). Importance of Critical Molecular Weight of Semicrystalline n-Type Polymers for Mechanically Robust, Efficient Electroactive Thin Films. *Chem. Mater.* 31, 3163–3173. <https://doi.org/10.1021/acs.chemmater.8b05114>.
  119. Peña-Alcántara, A., Nikzad, S., Michalek, L., Prine, N., Wang, Y., Gong, H., Ponte, E., Schneider, S., Wu, Y., Root, S.E., et al. (2023). Effect of Molecular Weight on the Morphology of a Polymer Semiconductor–Thermoplastic Elastomer Blend. *Adv. Electron. Mater.* 9, 2201055. <https://doi.org/10.1002/aeml.202201055>.
  120. Savagatrup, S., Makaram, A.S., Burke, D.J., and Lipomi, D.J. (2014). Mechanical properties of conjugated polymers and polymer-fullerene composites as a function of molecular structure. *Adv. Funct. Mater.* 24, 1169–1181. <https://doi.org/10.1002/adfm.201302646>.
  121. Ding, Y., Zhu, Y., Wang, X., Wang, Y., Zhang, S., Zhang, G., Gu, X., and Qiu, L. (2022). Side Chain Engineering: Achieving Stretch-Induced Molecular Orientation and Enhanced Mobility in Polymer Semiconductors. *Chem. Mater.* 34, 2696–2707. <https://doi.org/10.1021/acs.chemmater.1c04085>.
  122. Ding, Y., Yuan, Y., Wu, N., Wang, X., Zhang, G., and Qiu, L. (2021). Intrinsically Stretchable-Type Polymer Semiconductors through Side Chain Engineering. *Macromolecules* 54, 8849–8859. <https://doi.org/10.1021/acs.macromol.1c00936>.
  123. Zhang, S., Alesadi, A., Mason, G.T., Chen, K.L., Freychet, G., Galuska, L., Cheng, Y.H., St. Onge, P.B.J., Ocheje, M.U., Ma, G., et al. (2021). Molecular Origin of Strain-Induced Chain Alignment in PDPP-Based Semiconducting Polymeric Thin Films. *Adv. Funct. Mater.* 31, 2100161. <https://doi.org/10.1002/adfm.202100161>.
  124. Savagatrup, S., Printz, A.D., Wu, H., Rajan, K.M., Sawyer, E.J., Zaretski, A.V., Bettinger, C.J., and Lipomi, D.J. (2015). Viability of stretchable poly(3-heptylthiophene) (P3HpT) for organic solar cells and field-effect transistors. *Synth. Met.* 203, 208–214. <https://doi.org/10.1016/j.synthmet.2015.02.031>.
  125. Printz, A.D., Savagatrup, S., Burke, D.J., Purdy, T.N., and Lipomi, D.J. (2014). Increased elasticity of a low-bandgap conjugated copolymer by random segmentation for mechanically robust solar cells. *RSC Adv.* 4, 13635–13643. <https://doi.org/10.1039/C4RA00029C>.
  126. Kim, J.S., Kim, J.H., Lee, W., Yu, H., Kim, H.J., Song, I., Shin, M., Oh, J.H., Jeong, U., Kim, T.S., and Kim, B.J. (2015). Tuning Mechanical and Optoelectrical Properties of Poly(3-hexylthiophene) through Systematic Regioregularity Control. *Macromolecules* 48, 4339–4346. <https://doi.org/10.1021/acs.macromol.5b00524>.
  127. Lu, C., Lee, W.Y., Gu, X., Xu, J., Chou, H.H., Yan, H., Chiu, Y.C., He, M., Matthews, J.R., Niu, W., et al. (2017). Effects of Molecular Structure and Packing Order on the Stretchability of Semicrystalline Conjugated Poly(Tetrathienoacene-diketopyrrolopyrrole) Polymers. *Adv. Electron. Mater.* 3, 1–13. <https://doi.org/10.1002/aeml.201600311>.
  128. Zhao, Y., Zhao, X., Zang, Y., Di, C.A., Diao, Y., and Mei, J. (2015). Conjugation-break spacers in semiconducting polymers: Impact on polymer processability and charge transport properties. *Macromolecules* 48, 2048–2053. <https://doi.org/10.1021/acs.macromol.5b00194>.
  129. Savagatrup, S., Zhao, X., Chan, E., Mei, J., and Lipomi, D.J. (2016). Effect of Broken Conjugation on the Stretchability of Semiconducting Polymers. *Macromol. Rapid Commun.* 37, 1623–1628. <https://doi.org/10.1002/marc.201600377>.
  130. Oh, J.Y., Rondeau-Gagné, S., Chiu, Y.C., Chortos, A., Lissel, F., Wang, G.J.N., Schroeder, B.C., Kurosawa, T., Lopez, J., Katsumata, T., et al. (2016). Intrinsically stretchable and healable semiconducting polymer for organic transistors. *Nature* 539, 411–415. <https://doi.org/10.1038/nature20102>.

131. Mun, J., Ochiai, Y., Wang, W., Zheng, Y., Zheng, Y.Q., Wu, H.C., Matsuhisa, N., Higashihara, T., Tok, J.B.H., Yun, Y., and Bao, Z. (2021). A design strategy for high mobility stretchable polymer semiconductors. *Nat. Commun.* 12, 3572. <https://doi.org/10.1038/s41467-021-23798-2>.
132. Lu, N., Wang, X., Suo, Z., and Vlassak, J. (2007). Metal films on polymer substrates stretched beyond 50%. *Appl. Phys. Lett.* 91, 221909. <https://doi.org/10.1063/1.2817234>.
133. Rahbar, N., Wolf, K., Orana, A., Fennimore, R., Zong, Z., Meng, J., Papandreou, G., Maryanoff, C., and Soboyejo, W. (2008). Adhesion and interfacial fracture toughness between hard and soft materials. *J. Appl. Phys.* 104, 103533. <https://doi.org/10.1063/1.3021350>.
134. Hutchinson, J.W., and Suo, Z. (1991). Mixed Mode Cracking in Layered Materials. *Adv. Appl. Mech.* 29, 63–191. [https://doi.org/10.1016/S0065-2156\(08\)70164-9](https://doi.org/10.1016/S0065-2156(08)70164-9).
135. Beuth, J.L. (1992). Cracking of thin bonded films in residual tension. *Int. J. Solids Struct.* 29, 1657–1675. [https://doi.org/10.1016/0020-7683\(92\)90015-L](https://doi.org/10.1016/0020-7683(92)90015-L).
136. Charalambides, P.G., Cao, H.C., Lund, J., and Evans, A.G. (1990). DEVELOPMENT OF A TEST METHOD FOR MEASURING THE MIXED MODE FRACTURE RESISTANCE OF BIMATERIAL INTERFACES. *Mech. Mater.* 8, 269–283. [https://doi.org/10.1016/0167-6636\(90\)90047-J](https://doi.org/10.1016/0167-6636(90)90047-J).
137. Özcam, A.E., Efimenko, K., and Genzer, J. (2014). Effect of ultraviolet/ozone treatment on the surface and bulk properties of poly(dimethyl siloxane) and poly(vinylmethyl siloxane) networks. *Polymer (Guildf)* 55, 3107–3119. <https://doi.org/10.1016/j.polymer.2014.05.027>.
138. Efimenko, K., Wallace, W.E., and Genzer, J. (2002). Surface modification of Sylgard-184 poly(dimethyl siloxane) networks by ultraviolet and ultraviolet/ozone treatment. *J. Colloid Interface Sci.* 254, 306–315. <https://doi.org/10.1006/jcis.2002.8594>.
139. Xu, J., Wang, S., Wang, G.J.N., Zhu, C., Luo, S., Jin, L., Gu, X., Chen, S., Feig, V.R., To, J.W.F., et al. (2017). Highly stretchable polymer semiconductor films through the nanoconfinement effect. *Science* (1979) 355, 59–64. <https://doi.org/10.1126/science.aah4496>.
140. Shafe, A.A., Schrickx, H.M., Ding, K., Ade, H., and O'Connor, B.T. (2023). Rubber-Toughened Organic Solar Cells: Miscibility–Morphology–Performance Relations. *ACS Energy Lett.* 8, 3720–3726. <https://doi.org/10.1021/acsenergylett.3c01124>.
141. Delongchamp, D.M., Kline, R.J., Fischer, D.A., Richter, L.J., and Toney, M.F. (2011). Molecular characterization of organic electronic films. *Adv. Mater.* 23, 319–337. <https://doi.org/10.1002/adma.201001760>.
142. Rivnay, J., Mannsfeld, S.C.B., Miller, C.E., Salleo, A., and Toney, M.F. (2012). Quantitative determination of organic semiconductor microstructure from the molecular to device scale. *Chem. Rev.* 112, 5488–5519. <https://doi.org/10.1021/cr3001109>.
143. Vezie, M.S., Few, S., Meager, I., Pieridou, G., Dörling, B., Ashraf, R.S., Goñi, A.R., Bronstein, H., McCulloch, I., Hayes, S.C., et al. (2016). Exploring the origin of high optical absorption in conjugated polymers. *Nat. Mater.* 15, 746–753. <https://doi.org/10.1038/nmat4645>.
144. Menzel, M., Axer, M., Amunts, K., De Raedt, H., and Michielsen, K. (2019). Diattenuation Imaging reveals different brain tissue properties. *Sci. Rep.* 9, 1939. <https://doi.org/10.1038/s41598-019-38506-w>.
145. Nordén, B., and Kurucsev, T. (1994). Analysing DNA complexes by circular and linear dichroism. *J. Mol. Recognit.* 7, 141–155. <https://doi.org/10.1002/jmr.300070211>.
146. Brown, P.J., Thomas, D.S., Köhler, A., Wilson, J.S., Kim, J.S., Ramsdale, C.M., Sirringhaus, H., and Friend, R.H. (2003). Effect of interchain interactions on the absorption and emission of poly(3-hexylthiophene). *Phys. Rev. B* 67, 064203. <https://doi.org/10.1103/PhysRevB.67.064203>.
147. Persson, N.E., Engmann, S., Richter, L.J., and Delongchamp, D.M. (2019). In Situ Observation of Alignment Templating by Seed Crystals in Highly Anisotropic Polymer Transistors. *Chem. Mater.* 31, 4133–4147. <https://doi.org/10.1021/acs.chemmater.9b00888>.
148. Chabincyn, M.L. (2008). X-ray scattering from films of semiconducting polymers. *Polym. Rev.* 48, 463–492. <https://doi.org/10.1080/15583720802231734>.
149. Steele, J.A., Solano, E., Hardy, D., Dayton, D., Ladd, D., White, K., Chen, P., Hou, J., Huang, H., Saha, R.A., et al. (2023). How to GIWAXS: Grazing Incidence Wide Angle X-Ray Scattering Applied to Metal Halide Perovskite Thin Films. *Adv. Energy Mater.* 13, 2300760. <https://doi.org/10.1002/aenm.202300760>.
150. Cho, E., Risko, C., Kim, D., Gysel, R., Cates, N., Breiby, D.W., McGehee, M.D., Toney, M.F., Kline, R.J., and Bredas, J.L. (2012). Three-dimensional packing structure and electronic properties of biaxially oriented poly(2,5-bis(3-alkylthiophene-2-yl)thieno[3,2-b]thiophene) films. *J. Am. Chem. Soc.* 134, 6177–6190. <https://doi.org/10.1021/ja210272z>.
151. Schuettfort, T., Watts, B., Thomsen, L., Lee, M., Sirringhaus, H., and McNeill, C.R. (2012). Microstructure of polycrystalline PBTBT films: Domain mapping and structure formation. *ACS Nano* 6, 1849–1864. <https://doi.org/10.1021/nn2051295>.
152. Lee, M.J., Chen, Z., Pietro, R.d., Heeney, M., and Sirringhaus, H. (2013). Electrooptical spectroscopy of uniaxially aligned polythiophene films in field-effect transistors. *Chem. Mater.* 25, 2075–2082. <https://doi.org/10.1021/cm400266h>.
153. Delongchamp, D.M., Kline, R.J., Jung, Y., Germack, D.S., Lin, E.K., Moad, A.J., Richter, L.J., Toney, M.F., Heeney, M., and McCulloch, I. (2009). Controlling the orientation of terraced nanoscale “ribbons” of a poly(thiophene) semiconductor. *ACS Nano* 3, 780–787. <https://doi.org/10.1021/nn800574f>.
154. McBride, M., Persson, N., Keane, D., Bacardi, G., Reichmanis, E., and Grover, M.A. (2018). A Polymer Blend Approach for Creation of Effective Conjugated Polymer Charge Transport Pathways. *ACS Appl. Mater. Interfaces* 10, 36464–36474. <https://doi.org/10.1021/acsami.8b13255>.
155. Arnaud, D., Pandey, R.K., Miyajima, S., Nagamatsu, S., Prakash, R., Takashima, W., Hayase, S., and Kaneto, K. (2013). Fabrication of Large-scale Drop-cast Films of  $\pi$ -conjugated Polymers with Floating-film Transfer Method. *Trans. Mat. Res. Soc. Japan* 38, 305–308. <https://doi.org/10.14723/TMRSJ.38.305>.
156. Wang, H., Chen, L., Xing, R., Liu, J., and Han, Y. (2015). Simultaneous control over both molecular order and long-range alignment in films of the donor-acceptor copolymer. *Langmuir* 31, 469–479. <https://doi.org/10.1021/la5037772>.
157. Brinkmann, M., Chandezon, F., Pansu, R.B., and Julien-Rabant, C. (2009). Epitaxial growth of highly oriented fibers of semiconducting polymers with a shish-kebab-like superstructure. *Adv. Funct. Mater.* 19, 2759–2766. <https://doi.org/10.1002/adfm.200900966>.
158. Lee, M.J., Gupta, D., Zhao, N., Heeney, M., McCulloch, I., and Sirringhaus, H. (2011). Anisotropy of charge transport in a uniaxially aligned and chain-extended, high-mobility, conjugated polymer semiconductor. *Adv. Funct. Mater.* 21, 932–940. <https://doi.org/10.1002/adfm.201001781>.
159. Wang, S., Li, H., Zhao, K., Zhang, L., Zhang, Q., Yu, X., Tian, H., and Han, Y. (2022). Increasing the Charge Transport of P(NDI2OD-T2) by Improving the Polarization of the NDI2OD Unit along the Backbone Direction and Preaggregation via H-Bonding. *Macromolecules* 55, 2497–2508. <https://doi.org/10.1021/acs.macromol.1c02329>.
160. Wang, S., Zhao, K., Li, J., Yu, X., Zhang, Q., and Han, Y. (2024). Microstructural Evolution of P(NDI2OD-T2) Films with Different Molecular Weight during Stretching Deformation. *Macromol. Rapid Commun.* 45, 2300624. <https://doi.org/10.1002/marc.202300624>.
161. Biniak, L., Hamidi-Sakr, A., Grodd, L., Escoubas, S., Dappe, Y.J., Grigorian, S., Schmutz, M., and Brinkmann, M. (2018). Structure and Charge Transport Anisotropy of Polythieno[3,4-b]-Thiophene-co-Benzodithiophene (PTB7) Oriented by High-Temperature Rubbing. *Adv. Electron. Mater.* 4, 1–8. <https://doi.org/10.1002/aelm.201700480>.
162. Zhang, X., Hudson, S.D., Delongchamp, D.M., Gundlach, D.J., Heeney, M., and McCulloch, I. (2010). In-plane liquid crystalline texture of high-performance thienothiophene copolymer thin films. *Adv. Funct. Mater.* 20, 4098–4106. <https://doi.org/10.1002/adfm.201001232>.
163. Yasuda, T., Han, L., and Tsutsui, T. (2009). Fabrication of Stretch-Oriented Regioregular Poly(3-Hexylthiophene) film and Its Application to Organic Field-Effect Transistors. *J. Photopol. Sci. Technol.* 22, 713–717. <https://doi.org/10.2494/PHOTOPOLYMER.22.713>.

164. Yasuda, T. (2011). Anisotropic carrier transport properties of stretch-oriented  $\pi$ -conjugated polymers in organic field-effect transistors. *Phys. Status Solidi* 8, 604–606. <https://doi.org/10.1002/pssc.201000405>.
165. Wu, H.C., Benight, S.J., Chortos, A., Lee, W.Y., Mei, J., To, J.W.F., Lu, C., He, M., Tok, J.B.-H., Chen, W.C., and Bao, Z. (2014). A rapid and facile soft contact lamination method: Evaluation of polymer semiconductors for stretchable transistors. *Chem. Mater.* 26, 4544–4551. <https://doi.org/10.1021/cm502271j>.
166. Scott, J.I., Xue, X., Wang, M., Kline, R.J., Hoffman, B.C., Dougherty, D., Zhou, C., Bazan, G., and O'Connor, B.T. (2016). Significantly Increasing the Ductility of High Performance Polymer Semiconductors through Polymer Blending. *ACS Appl. Mater. Interfaces* 8, 14037–14045. <https://doi.org/10.1021/acsami.6b01852>.
167. Ocheje, M.U., Selivanova, M., Zhang, S., Van Nguyen, T.H., Charron, B.P., Chuang, C.H., Cheng, Y.H., Billet, B., Noori, S., Chiu, Y.C., et al. (2018). Influence of amide-containing side chains on the mechanical properties of diketopyrrolopyrrole-based polymers. *Polym. Chem.* 9, 5531–5542. <https://doi.org/10.1039/c8py01207e>.
168. Dyreklev, P., Berggren, M., Inganäs, O., Andersson, M.R., Wennerström, O., and Hjertberg, T. (1995). Polarized electroluminescence from an oriented substituted polythiophene in a light emitting diode. *Adv. Mater.* 7, 43–45. <https://doi.org/10.1002/adma.19950070108>.
169. Lemmer, U., Vacar, D., Moses, D., Heeger, A.J., Ohnishi, T., and Noguchi, T. (1996). Electroluminescence from poly(phenylene vinylene) in a planar metal-polymer-metal structure. *Appl. Phys. Lett.* 68, 3007–3009. <https://doi.org/10.1063/1.116679>.
170. Bradley, D.D.C., Friend, R.H., Lindenberg, H., and Roth, S. (1986). Infra-red characterization of oriented poly(phenylene vinylene). *Polymer (Guildf)* 27, 1709–1713. [https://doi.org/10.1016/0032-3861\(86\)90265-X](https://doi.org/10.1016/0032-3861(86)90265-X).
171. Gao, Y., Liao, J., Chen, H., Ning, H., Wu, Q., Li, Z., Wang, Z., Zhang, X., Shao, M., and Yu, Y. (2023). High Performance Polarization-Resolved Photodetectors Based on Intrinsically Stretchable Organic Semiconductors. *Adv. Sci.* 10, e2204727–e2204729. <https://doi.org/10.1002/advs.202204727>.
172. Zhu, R., Kumar, A., and Yang, Y. (2011). Polarizing organic photovoltaics. *Adv. Mater.* 23, 4193–4198. <https://doi.org/10.1002/adma.201101514>.
173. Tanaka, H., Yasuda, T., Fujita, K., and Tsutsui, T. (2006). Transparent image sensors using an organic multilayer photodiode. *Adv. Mater.* 18, 2230–2233. <https://doi.org/10.1002/adma.200600163>.
174. Matsushima, T., Matsuo, H., Yamamoto, T., Nakao, A., and Murata, H. (2014). Horizontally oriented molecular thin films for application in organic solar cells. *Sol. Energy Mater. Sol. Cell.* 123, 81–91. <https://doi.org/10.1016/j.solmat.2014.01.004>.
175. Altaqui, A., Sen, P., Schrickx, H., Rech, J., Lee, J.W., Escuti, M., You, W., Kim, B.J., Kolbas, R., O'Connor, B.T., and Kudenov, M. (2021). Mantis shrimp-inspired organic photodetector for simultaneous hyperspectral and polarimetric imaging. *Sci. Adv.* 7, eabe3196. <https://doi.org/10.1126/sciadv.abe3196>.
176. Altaqui, A., Schrickx, H., Sen, P., Li, L., Rech, J., Lee, J.-W., Balar, N., You, W., Kim, B.J., Escuti, M., et al. (2021). Bio-inspired spectropolarimetric sensor based on tandem organic photodetectors and multi-twist liquid crystals. *Opt Express* 29, 43953. <https://doi.org/10.1364/oe.431858>.
177. Huh, Y.H., Bae, I.-G., Jeon, H.G., and Park, B. (2016). Homogeneous PCBM layers fabricated by horizontal-dip coating for efficient bilayer heterojunction organic photovoltaic cells. *Opt Express* 24, A1321–A1335. <https://doi.org/10.1364/oe.24.0a1321>.
178. Siddika, S., Peng, Z., Balar, N., Dong, X., Zhong, X., You, W., Ade, H., and O'Connor, B.T. (2023). Molecular interactions that drive morphological and mechanical stabilities in organic solar cells. *Joule* 7, 1593–1608. <https://doi.org/10.1016/j.joule.2023.06.002>.
179. Peng, Z., Xian, K., Cui, Y., Qi, Q., Liu, J., Xu, Y., Chai, Y., Yang, C., Hou, J., Geng, Y., and Ye, L. (2021). Thermoplastic Elastomer Tunes Phase Structure and Promotes Stretchability of High-Efficiency Organic Solar Cells. *Adv. Mater.* 33, e2106732. <https://doi.org/10.1002/adma.202106732>.
180. Döring, B., Sánchez-Díaz, A., Arteaga, O., Veciana, A., Alonso, M.I., and Campoy-Quiles, M. (2017). Controlled Pinning of Conjugated Polymer Spherulites and Its Application in Detectors. *Adv. Opt. Mater.* 5, 1700276. <https://doi.org/10.1002/adom.201700276>.
181. Yang, R., Sen, P., O'Connor, B.T., and Kudenov, M.W. (2020). Optical crosstalk and off-axis modeling of an intrinsic coincident polarimeter. *Appl. Opt.* 59, 156–164. <https://doi.org/10.1364/ao.59.000156>.
182. Yang, R., Sen, P., O'Connor, B., and Kudenov, M. (2020). Optimization of an intrinsic coincident polarimeter and quantitative architectural comparison of different polarimeter techniques. *Opt. Eng.* 59, 1. <https://doi.org/10.1117/1.oe.59.2.024111>.
183. Tyo, J.S., Goldstein, D.L., Chenault, D.B., and Shaw, J.A. (2006). Review of passive imaging polarimetry for remote sensing applications. *Appl. Opt.* 45, 5453–5469. <https://doi.org/10.1364/AO.45.005453>.
184. Bueno, J.M., and Artal, P. (1999). Double-pass imaging polarimetry in the human eye. *Opt. Lett.* 24, 64–66. <https://doi.org/10.1364/ol.24.000064>.